Soils and Foundations 2012;52(2):279–298

The Japanese Geotechnical Society

Soils and Foundations

www.sciencedirect.com
journal homepage: www.elsevier.com/locate/sandf

Parameter identification for Cam-clay model in partial loading model tests using the particle filter

Takayuki Shuku[a,*], Akira Murakami[b], Shin-ichi Nishimura[a], Kazunori Fujisawa[a], Kazuyuki Nakamura[c]

[a]*Graduate School of Environmental and Life Science, Okayama University, 3-1-1 Tsushimanaka, Kita-ku, Okayama 700-8530 Japan*
[b]*Graduate School of Agriculture, Kyoto University, Kitashirakawa-oiwakecho, Sakyo-ku, Kyoto 606-8502 Japan*
[c]*Graduate School of Advanced Mathematical Sciences, Meiji University, 1-1-1 Higashimita, Tama-ku, Kawasaki 214-8571, Japan*

Available online 29 March 2012

Abstract

Data assimilation is a versatile methodology, developed in the earth sciences, such as geophysics, meteorology, and oceanography, for estimating the state of a dynamic system of interest by merging sparse observation data into a numerical model for the system. In particular, the data assimilation method referred to as the particle filter (PF) can be applied to nonlinear and non-Gaussian problems, and it holds the greatest potential for application to geotechnical problems. The objective of this study is to demonstrate the theoretical and the practical effectiveness of the PF for a geotechnical problem, i.e., applying the methodology to numerical experiments and actual model tests to identify the parameters of elasto-plastic geomaterials. Since the mechanical behavior of soils depends on both the current stress and the recent stress history of the soil, the sampling method called SIS, which can take into account the stress history experienced by soils, identifies the parameters of elasto-plastic geomaterials remarkably well. The results of the numerical tests have shown that the parameters identified by the PF based on the SIS have converged into their true values, and the approach presented in this study has shown great promise as an accurate parameter identification method for elasto-plastic geomaterials. Moreover, the simulation results using the identified parameters were close to the actual measurement data, and long-term predictions with high accuracy could be achieved, even though short-term measurement data were used. The PF approach produces more information about the parameters of interest than simple estimated values obtained from optimization methods. Namely, the identification comes in the form of probability density functions.

Keywords: Data assimilation; Inverse analysis; Parameter identification; Particle filter; Cam-clay model; Soil–water coupled finite element analysis (IGC:E2/E13)

1. Introduction

Prediction has always played a significant role in nearly every aspect of construction projects for geotechnical infrastructures. Geotechnical engineers, however, have to do more than make predictions: they are responsible for deciding the most appropriate actions to be taken based on these predictions in order to realize maximum economy and safety assurance. The development of the computer has greatly improved prediction capabilities, since it allows enormous quantities of data to be handle, and has enabled the use of numerical simulations for making predictions in geotechnical engineering for such works as shallow/deep foundations, tunnels, cut slopes, and road/railway embankments.

*Corresponding author.
E-mail address: shuku@cc.okayama-u.ac.jp (T. Shuku).

0038-0806

Peer review under responsibility of The Japanese Geotechnical Society
doi:10.1016/j.sandf.2012.02.006

In spite of the great number of discussions and research works, discrepancies between the predictions made using sophisticated simulation techniques and the observation data continue to exist (e.g., Brand and Premchitt, 1989). Laboratory or *in situ* tests can be used to obtain the soil parameters required for the various predictive methods. In practice, however, obtaining accurate parameters is a difficult task because of the many sources of uncertainty in geotechnical analyses. To make matters worse, soils, which are products of natural processes, are highly variable and display very complex behavior. Consequently, geotechnical engineers must make decisions based on incomplete information.

To cope with the above uncertainties, inverse analysis techniques have been proposed and applied to geotechnical problems for the past three decades. These techniques are used more and more frequently in geotechnical practices, e.g., tunnel excavations in rock (Sakurai and Takeuchi, 1983; Karakus and Fowell, 2005), embankments on soft grounds (Asaoka, 1978; Arai et al., 1984, 1986, 1987; Murakami and Hasegawa, 1987; Nishimura et al., 2002, 2005), single-pile settlement (e.g., Honjo et al., 1993), and excavations with support systems (Finno and Calvello, 2005; Rechae et al., 2008). Gioda and Sakurai (1987) reviewed some developments of the numerical techniques for inverse analysis in the field of geomechanics over the past few decades.

Inverse analyses have been successfully applied to linear elastic problems in which the deformation to be addressed is linear and depends only on the model parameters and the applied load; it does not depend on the loading history. However, the mechanical behavior of geomaterials is commonly described by an elasto-plastic model, and recent sophisticated constitutive models for soils have been formulated on the basis of the elasto-plastic theory (e.g., Asaoka et al., 2002; Nakai and Hinokio, 2004). The deformation behavior of elasto-plastic geomaterials displays strong nonlinearity and depends not only on the values of the parameters, but also to a great extent on the stress state and the history, whereby the parameter identification of elasto-plastic models still remains a major challenge.

Data assimilation (DA) is available as a methodology to overcome the above difficulties (Nakamura et al., 2005). The estimation of the interest dynamic system via DA involves a combination of observation data and the underlying dynamical principles governing the system. The melding of data and dynamics has produced a powerful methodology which makes efficient and realistic estimations possible. This approach has recently proven fruitful in the earth sciences, e.g., geophysics, meteorology, and oceanography (e.g., Awaji et al., 2009). The discipline of geotechnical engineering is no exception; the concept of DA has been given much attention, and has been applied to some geotechnical problems since the 1980s. A pioneering work of DA strategy in geomechanics includes the literature of Murakami and Hasegawa (1985) and Murakami (1991), who applied the Kalman filter (KF) and the extended Kalman filter (EKF), which assimilate observation data into simulation models, to identify and estimate problems in geomechanics.

Several kinds of powerful DA methods, such as 4D-VAR (Talagrand and Courtier, 1987), the representer method (Bennett, 1992, 2002), and the ensemble Kalman filter method (EnKF) (Evensen, 1994), have been proposed. Among the existing strategies, this study focuses on the filtering techniques referred to as the PF (Gordon et al., 1993; Kitagawa, 1996; Higuchi, 2005). The PF can be applied to nonlinear and non-Gaussian problems and can provide a simple conceptual formulation and ease of implementation. It has been used extensively in ocean and atmospheric science, oil reservoir simulations, and hydrological modeling (e.g., Nakamura et al., 2006; Nakano et al., 2007; Awaji et al., 2009). Clearly, the PF holds the greatest potential for application in geotechnical engineering, and existing technical issues in geomechanics can be overcome through its use.

The objective of this study is to demonstrate the theoretical and practical effectiveness of the DA method, i.e., the PF, for the parameter identification of elasto-plastic models, by applying the methodology to numerical experiments and actual model tests. First, an overview of the concepts and methods of data assimilation is presented, and the potential of the PF for use in geomechanics is discussed, with its formulation and algorithm explained. Then, the PF is applied to numerical tests, where material parameters of the elasto-plastic geomaterial, i.e., the Cam-clay model, are identified by simulating the shear behavior of soil elements under undrained or drained conditions, and the suitability of the PF is examined. Finally, an application example of the PF to an actual model test is shown, and its practical capability is discussed. The deformational behavior of a clay block sample, partially loaded, is simulated by a finite element analysis with the Cam-clay model, for which the elasto-plastic parameters are identified using the PF. Then, whether or not the finite element analyses using the identified parameters produce accurate simulations is investigated.

2. DA using the PF

2.1. Concepts and methods of DA

DA is a versatile methodology for estimating the state of a dynamic system of interest by merging sparse observation data into a numerical model for the system. The state of the system is usually estimated with deterministic simulation models, which are subject to the uncertainty that arises due to a lack of knowledge and a poor understanding of the physical phenomena. Meanwhile, observation data, which represent the true state but are subject to stochastic uncertainty and randomness, may occasionally be available as a function of a subset of the system variables. Based upon a prognostic model and a

limited number of observations, DA attempts to provide a more comprehensive system analysis which may lead to more accurate predictions.

DA methods can be split into two different categories, according to the way the updating is done with regard to time:

1) *Variational data assimilation*: Past observations, from the start of the modeling until the present time, are used simultaneously to correct the initial conditions of the model and to obtain the best overall fit of the state to the observations. The concept of variational data assimilation methods is shown in Fig. 1. The methods minimize the squared distance between the analysis and the background state at the beginning of the assimilation, and between observations (symbols) and the forecast run (the continuous lines) throughout the assimilation.
2) *Sequential data assimilation*: Observations are used as soon as they are available to correct the present state of the model. The concept is illustrated in Fig. 2. In contrast to variational methods, sequential methods lead to discontinuities in the time series of the corrected state. When an observation becomes available, the model forecast (continuous line) is updated to a value closer to the observation (symbol) that is used to make the next model forecast.

Variational DA methods include 4D-VAR (e.g., Talagrand and Courtier, 1987) and the representer method (Bennett, 1992, 2002). In particular, 4D-VAR is a novel technique, which has recently been applied to weather forecasts (e.g., Yumimoto, 2009). On the other hand, sequential DA methods include the KF (Kalman, 1960), the EKF (Katayama, 1983), the EnKF (Evensen, 1994), and the PF (Gordon et al., 1993; Kitagawa, 1996). The KF and the EKF, which is a nonlinear version of the KF, are well-known DA techniques; they have been used not only in earth science, but also in geotechnical engineering (e.g., Murakami and Hasegawa, 1985, 1993; Suzuki and Ishii, 1994). The EnKF and the PF are based on the Monte Carlo approach to approximating the state probability distribution by a finite number of independent model trajectories, also called particles or realizations. Both methods, therefore, are called ensemble-based filters.

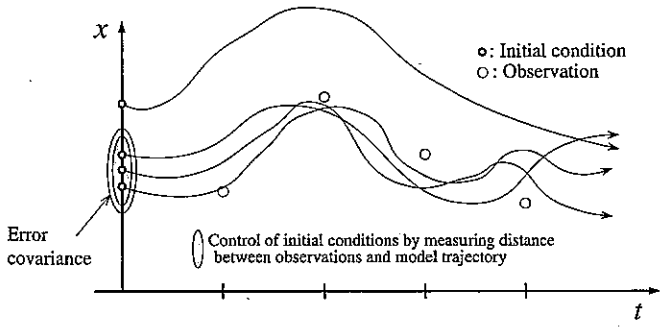

Fig. 1. Concept of variational data assimilation.

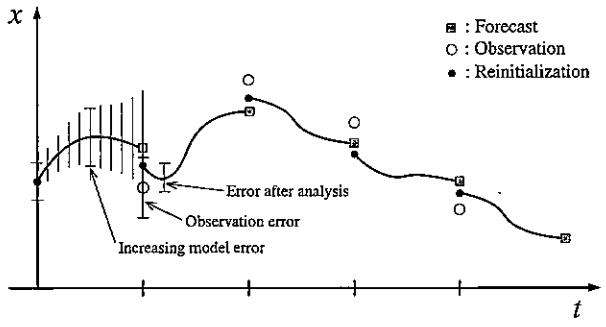

Fig. 2. Concept of sequential data assimilation.

This study focuses on the PF and applies it to parameter identification problems in geomechanics. The sequential approach produces more information about the parameters of interest than simple estimated values obtained from a variational DA method, namely, the identification comes in the form of probability density functions (PDFs). As noted above, novel sequential DA methods include the EnKF and the PF. Although the EnKF can be applied to nonlinear systems, it basically assumes a linear relationship between a state and the observation data in calculating a Kalman gain. Therefore, the EnKF cannot produce satisfactory estimates if its linear approximation is invalid. This means that its application to geomaterials is difficult, because the materials display strong nonlinearity. On the other hand, as the PF does not require assumptions of linearity or Gaussianity, it is applicable to general problems. In addition, the PF uses the recursive formula of the sequential Bayesian framework directly and approximates the posterior probability distributions by means of appropriate weights associated with each realization. In contrast to the EnKF, the PF makes no assumptions regarding the formula for the prior distribution of the model state; as such, convergence to the true state is ensured for a sufficiently large ensemble size. Therefore, the PF has high potential for application to geotechnical engineering and can achieve fruitful outcomes. This section provides a thorough description of the PF.

2.2. Nonlinear non-Gaussian state space model and state estimation

We consider a nonlinear and non-Gaussian state space model, which is represented in the following (Kitagawa, 1987):

$$x_t = f_t(x_{t-1}) + v_t \tag{1}$$

$$y_t = h_t(x_t) + w_t \tag{2}$$

where $x_t=(x_1, x_2, \ldots, x_k)$ and $y_t=(y_1, y_2, \ldots, y_l)$ represent the state vector and the observation vector, respectively, and subscripts k and l are the dimension of state vectors and observation vectors, respectively; f_t and h_t are the nonlinear dynamic model operator and the observation operator, respectively. Subscript t denotes the discrete time

index. Vectors v_t and w_t refer to the system error vector and the observation error vector, respectively, whose PDF follows the normal distribution with zero mean, namely

$$v_t \sim N(0, Q_t) \tag{3}$$

$$w_t \sim N(0, R_t) \tag{4}$$

where Q_t and R_t are predetermined covariance matrices.

This study focuses on the mechanical behavior of geomaterials, which can be described by soil–water coupled finite element techniques. By means of the formulation of the soil–water coupled FEM, Eq. (1) can be rewritten in the following form:

$$\begin{Bmatrix} u_t \\ p_t \end{Bmatrix} = \begin{Bmatrix} u_{t-1} \\ p_{t-1} \end{Bmatrix} + \begin{bmatrix} [K] & [K_v]^T \\ [K_v] & -\theta\Delta t[K_h] \end{bmatrix}^{-1} \times \begin{Bmatrix} \{\dot{F}\} + [K_v]^T p_t \\ \{\dot{Q}\} + (1-\theta)[K_h]p_t \end{Bmatrix} + \begin{Bmatrix} v_t^u \\ v_t^p \end{Bmatrix} \tag{5}$$

where the following notations are employed: $[K]$ is the tangent stiffness matrix of the soil skeleton which is modeled by constitutive models for soils, $[K_v]$ is the rectangular matrix that transforms the increment in nodal displacements to the volume change of each element, $[K_v]^T$ is the transpose of $[K_v]$ that transforms the pore pressure of an element to the seepage force of element, $[K_h]$ is the fluid stiffness matrix, $\{\dot{F}\}$ is a vector that represents the increment in applied force, $\{u_t\}$ is the nodal displacement vector at time t, $\{p_t\}$ is the nodal pore pressure vector at time t, θ is the time-varying coefficient, $(0 < \theta < 1)$, $\{\dot{Q}\}$ is the vector that represents the increment in the volume rate of the water flow, $\{v_t^u\}$ is the system error vector for $\{u_t\}$, $\{v_t^p\}$ is the system error vector for $\{p_t\}$.

Thus, state vector x_t is constructed as

$$x_t = \begin{Bmatrix} u_t \\ p_t \end{Bmatrix} \tag{6}$$

If state variables u_1, u_2, and u_3 in $\{u_t\}$ are directly observed, nonlinear function h_t can be written in matrix form as

$$H_t = \begin{bmatrix} 1 & 0 & 0 & \cdots & 0 \\ 0 & 1 & 0 & \cdots & 0 \\ 0 & 0 & 1 & \cdots & 0 \end{bmatrix} \tag{7}$$

We can describe $y_t = H_t x_t$ using the above matrix.

The recursive formula for obtaining a one-step-ahead prediction and filtering densities can be derived as follows:

One-step-ahead prediction (time update)

$$\begin{aligned} p(x_t|y_{1:t-1}) &= \int_{-\infty}^{\infty} p(x_t, x_t|y_{1:t-1})dx_{t-1} \\ &= \int_{-\infty}^{\infty} p(x_t|x_{t-1}, y_{1:t-1})p(x_{t-1}|y_{1:t-1})dx_{t-1} \\ &= \int_{-\infty}^{\infty} p(x_t|x_{t-1})p(x_{t-1}|y_{1:t-1})dx_{t-1} \end{aligned} \tag{8}$$

Filtering (observation update)

$$\begin{aligned} p(x_t|y_{1:t}) &= \frac{p(x_t, y_t|y_{1:t-1})}{p(y_t|y_{1:t-1})} = \frac{p(y_t|x_t, y_{1:t-1})\cdot p(x_t|y_{1:t-1})}{p(y_t|y_{1:t-1})} \\ &= \frac{p(y_t|x_t)\cdot p(x_t|y_{1:t-1})}{p(y_t|y_{1:t-1})} \end{aligned} \tag{9}$$

where $p(x_t|x_{t-1})$ is the density of x_t given previous state vector x_{t-1}, $p(y_t|x_t)$ is the density of y_t given x_t, and $p(y_t|y_{1:t-1})$ is obtained by $\int p(y_t|x_t)p(x_t|y_{1:t-1})dx_t$.

In practice, computing Eqs. (8) and (9) is difficult, because analytical solutions are available in only a few stylized cases, which include the linear and the Gaussian models. In the Gaussian case, the KF provides deterministic updating recursions. Therefore, in both nonlinear and non-Gaussian cases, numerical techniques such as the PF must be employed.

2.3. PF

The PF approximates PDFs via a set of realizations called an ensemble that has weights, and each realization is referred to as a 'particle' or a 'sample'. For example, a filtered distribution at time $t-1$, $p(x_{t-1}|y_{1:t-1})$, where $y_{1:t-1}$ denotes $\{y_1, y_2, \ldots, y_{t-1}\}$, is approximated with ensemble $\{x^{(1)}_{t-1|t-1}, x^{(2)}_{t-1|t-1}, \ldots, x^{(N)}_{t-1|t-1}\}$ and weights $\{w^{(1)}_{t-1}, w^{(2)}_{t-1}, \ldots, w^{(N)}_{t-1}\}$ by the following equation:

$$p(x_{t-1}|y_{1:t-1}) \approx \frac{1}{N}\sum_{i=1}^{N} w^{(i)}_{t-1}\delta(x_{t-1} - x^{(i)}_{t-1|t-1}) \tag{10}$$

where N is the number of particles and δ is the Dirac delta function, $w^{(i)}_{t-1}$ is the weight attached to particles $x^{(i)}_{t-1|t-1}$ and should suffice $w^{(i)}_{t-1} \geq 0$ and $\sum_{i=1}^{N} w^{(i)}_{t-1} = 1$. Given the particle approximation, Eqs. (8) and (9) become a sum instead of an integral.

We obtain the ensemble approximation for the forecast distribution $p(x_t|y_{1:t-1})$ at time t from the Eqs. (8) and (10) by the following calculation:

$$\begin{aligned} p(x_t|y_{1:t-1}) &= \int_{-\infty}^{\infty} p(x_t|x_{t-1})p(x_{t-1}|y_{1:t-1})dx_{t-1} \\ &\approx \sum_{i=1}^{N}\int_{-\infty}^{\infty} w^{(i)}_{t-1}\delta(x_{t-1} - x^{(i)}_{t-1|t-1})p(x_t|x_{t-1})dx_{t-1} \\ &= \sum_{i=1}^{N} w^{(i)}_{t-1}\delta(x_t - f_t(x^{(i)}_{t-1|t-1}, v^{(i)}_t)) \\ &= \sum_{i=1}^{N} w^{(i)}_{t-1}\delta(x_t - x^{(i)}_{t|t-1}) \end{aligned} \tag{11}$$

where, $\{v^{(i)}_t\}_{i=1}^{N}$ is an i.i.d. sample set for Eq. (3). The calculation means that each particle for the prediction ensemble, $x^{(i)}_{t|t-1}$, is obtained by the direct calculation of $f_t(x^{(i)}_{t-1|t-1}, v^{(i)}_t)$.

On the other hand, we obtain the ensemble approximation for filtered distribution $p(x_t|y_{1:t})$, from Eqs. (9) and (11), and observation y_t by the following calculation:

$$\begin{aligned} p(x_t|y_{1:t}) &= \frac{p(y_t|x_t)\cdot p(x_t|y_{1:t-1})}{p(y_t|y_{1:t-1})} \\ &= \frac{p(y_t|x_t)\cdot p(x_t|y_{1:t-1})}{\int_{-\infty}^{\infty} p(y_t|x_t)\cdot p(x_t|y_{1:t-1})dx_t} \\ &= \frac{1}{\sum_j p(y_t|x_{t|t-1}^{(j)})w_{t-1}^{(j)}} \sum_{i=1}^{N} p(y_t|x_{t|t-1}^{(i)}) \\ &\quad \times w_{t-1}^{(i)}\delta(x_t - x_{t|t-1}^{(i)}) \\ &= \sum_{i=1}^{N} \tilde{w}_t^{(i)} w_{t-1}^{(i)} \delta(x_t - x_{t|t-1}^{(i)}) \\ &= \sum_{i=1}^{N} w_t^{(i)} \delta(x_t - x_{t|t-1}^{(i)}) \end{aligned} \tag{12}$$

where $\tilde{w}_t^{(i)}$ is defined as

$$\tilde{w}_t^{(i)} = \frac{p(y_t|x_{t|t-1}^{(i)})}{\sum_j p(y_t|x_{t|t-1}^{(j)})w_{t-1}^{(j)}} \tag{13}$$

If the observation system is linear, $p(y_t|x_{t|t-1}^{(i)})$ is given as follows:

$$p(y_t|x_{t|t-1}^{(i)}) = \frac{1}{(2\pi)^{m/2}|R_t|} \times \exp\left[\frac{-(y_t - H_t(x_{t|t-1}^{(i)}))^{\mathrm{T}} R_t^{-1} (y_t - H_t(x_{t|t-1}^{(i)}))}{2}\right] \tag{14}$$

where m is the number of state variables. Each weight $w_t^{(i)}$ is the product of $\tilde{w}_t^{(i)}$ and the previous time weight, namely

$$w_t^{(i)} = \tilde{w}_t^{(i)} w_{t-1}^{(i)} \tag{15}$$

2.4. Sampling methods

The central problem in particle filtering is how to sample from $p(x_t|y_{1:t})$. A particle filtering algorithm essentially consists of different ways of sampling. We now discuss a number of prominent particle filtering algorithms. The differences between sampling importance resampling (SIR) and sequential importance sampling (SIS) are shown, and their applicability to geotechnical problems is discussed.

The classic particle filtering algorithm is known as the SIR algorithm (Gordon et al., 1993; Kitagawa, 1996). The algorithm of SIR is summarized as follows:

1. Initialization:
   Generate an ensemble (set of particles) $\{x_0^{(1)}, x_0^{(2)}, \ldots, x_0^{(N)}\}$ from the initial distribution $p(x_0)$. Set $t=1$.
2. Prediction:
   Each particle $x_{t-1}^{(i)}$ evolves according to the numerical dynamic model given by Eq. (1).
3. Filtering:
   After obtaining measurement data y_t, calculate weight $w_t^{(i)}$, which expresses the "fitness" of the prior particles to the observation data, and assign a weight, $\tilde{w}_t^{(i)}$, to each $x_{t-1}^{(i)}$.
4. Resampling:
   Generate new particles $\{x_t^{(1)}, x_t^{(2)}, \ldots, x_t^{(N)}\}$ by resampling N times from the set of particles $x_{t-1}^{(i)}$, which is obtained in the filtering stage, where $\Pr(x_t^{(j)} = x_{t-1}^{(i)}) = w_t^{(i)}$ and set weight $w_t^{(j)} = 1/N$. The set of determined particles $\{x_t^{(i)}\}$ results in an ensemble approximation of filtered distribution $p(x_t|y_{1:t})$.
   Set $t=t+1$ and go back to Step 2.

On the other hand, a general approach for filtering is known as SIS (Doucet et al., 2000; Moral et al., 2006). The SIS algorithm can be viewed as a generalization of the SIR algorithm; it is based on using the importance sampling to estimate the expectations of functions of the state variables. The algorithm of SIS is summarized as follows:

1. Initialization:
   Generate an ensemble (set of particles) $\{x_0^{(1)}, x_0^{(2)}, \cdots, x_0^{(N)}\}$ from the initial distribution $p(x_0)$.
2. Prediction:
   Each particle $x_{t-1}^{(i)}$ evolves according to the numerical dynamic model given by Eq. (1).
3. Filtering:
   After obtaining measurement data y_t, calculate weight $w_t^{(i)}$, which expresses the "fitness" of the prior particles to the observation data computed by Eq. (13), and assign a weight, $w_t^{(i)}$, to each $x_{t-1}^{(i)}$.
4. Weight update:
   The set of weighted particles $\{x_t^{(i)}\}$ results in an ensemble approximation of filtered distribution $p(x_t|y_{1:t})$.
   Set $t=t+1$ and go back to Step 2.

Fig. 3 shows the two discrete approximations for a PDF by SIR and SIS.

The question now is which sampling method is preferable for geotechnical problems. Let us focus on the mechanical behavior of soil herein. Soil undergoes both elastic and plastic deformation when subjected to loading and is said to be in the critical state when it undergoes larger shear deformation at constant volume, constant shear and normal effective stress conditions (Schofield and Wroth, 1968). The mechanical behavior can be clearly described by the critical state constitutive models, e.g., the Cam-clay model and the Sekiguchi-Ohta model. In the critical state theory, the state of a soil is described by the current values of stress parameters q and p' and the specific volume $(1+e)$. The consolidation history of soil is described by the overconsolidation ratio $\mathrm{OCR} = p'_m/p'$ where p'_m is the stress at the intersection of the current swelling line with the normal consolidation line, as shown

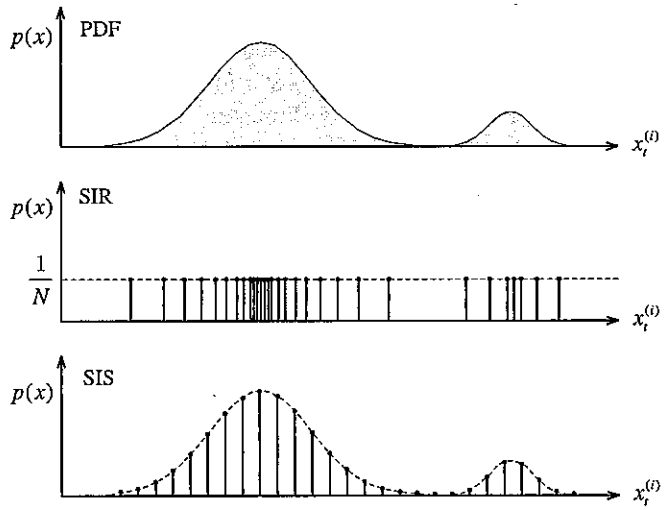

Fig. 3. Filtered PDF approximated by the particles.

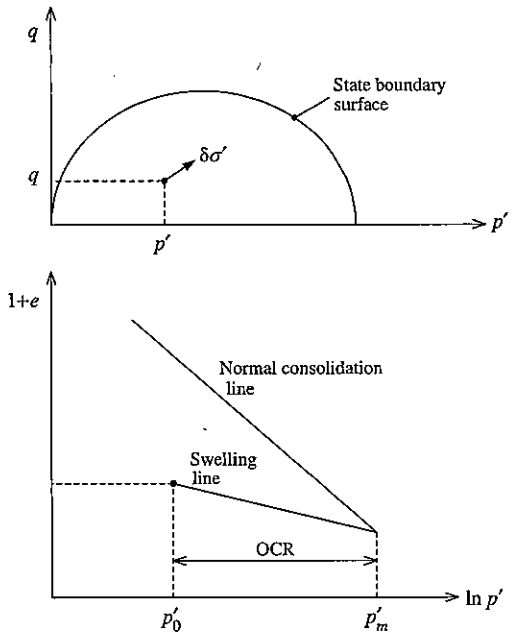

Fig. 4. Current stress and consolidation history (modified from Atkinson et al., 1990).

in Fig. 4. In many relatively simple theories for stress–strain behavior, such as the Cam-clay model, the value of p'_m defines the size of the state boundary surface which separates the elastic states inside from the elasto-plastic states on the boundary surface.

It is well known that the stress–strain response of a soil not only depends on the current stress, but also on the recent stress history of the soil (Atkinson et al., 1990). In most current theories for soils, the stress–strain behavior is taken to depend principally on the current state and on the consolidation history defined by the overconsolidation ratio. Problems involving unidirectional stress paths, such as one-dimensional consolidation, may be described by a simple nonlinear elasto-plastic model. However, for situations where the stress path directions may vary due to either the stress history or loading, a strain-dependent nonlinear elasto-plastic model is desirable. The magnitude of the effect of the recent history is determined largely by the difference in the direction of loading between the current and the previous stress paths. The effect of the stress history is illustrated in Fig. 5. Samples brought to the same initial states of q_i and p_i at zero, and along the different paths of CO and DO, are then loaded along the same path, OA. Fig. 5(b) illustrates the stress–strain curves for the same loading path OA. Soil offers resistance to change in the direction of loading, which implies that the stress–strain behavior of the current stress path depends on the stress history. Since the samples had identical states and over-consolidation ratios at O, and assuming that they were both held at this state for equal periods of time, the difference in stiffness is attributable to the difference in stress histories. Soil offers resistance to change in the direction of loading, which implies that the stress–strain behavior of the current stress path depends on the stress history of the soil.

As noted above, the stress/loading history is an important factor for evaluating the mechanical behavior of soils. Let us focus on both of the sampling methods again; the SIR algorithm cannot take into account the stress history the soils have experienced since it generates new particles based on the observation data during the assimilation. On the other hand, the SIS algorithm keeps the initially generated particles, i.e., the geotechnical parameters, constant during the entire process of filtering, and their weights are updated simply based on the sequentially observed data. This means that the SIS algorithm can accomplish the task of evaluating of the mechanical behavior of soils after taking into account the stress history, and it can produce accurate data assimilation in geotechnical problems. The algorithms of the PF are shown in Fig. 6.

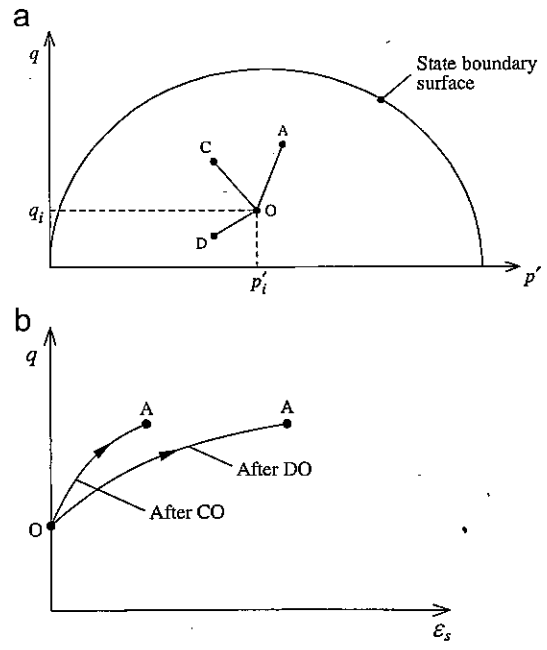

Fig. 5. Effect of recent stress history on current stiffness (modified from Atkinson et al., 1990).

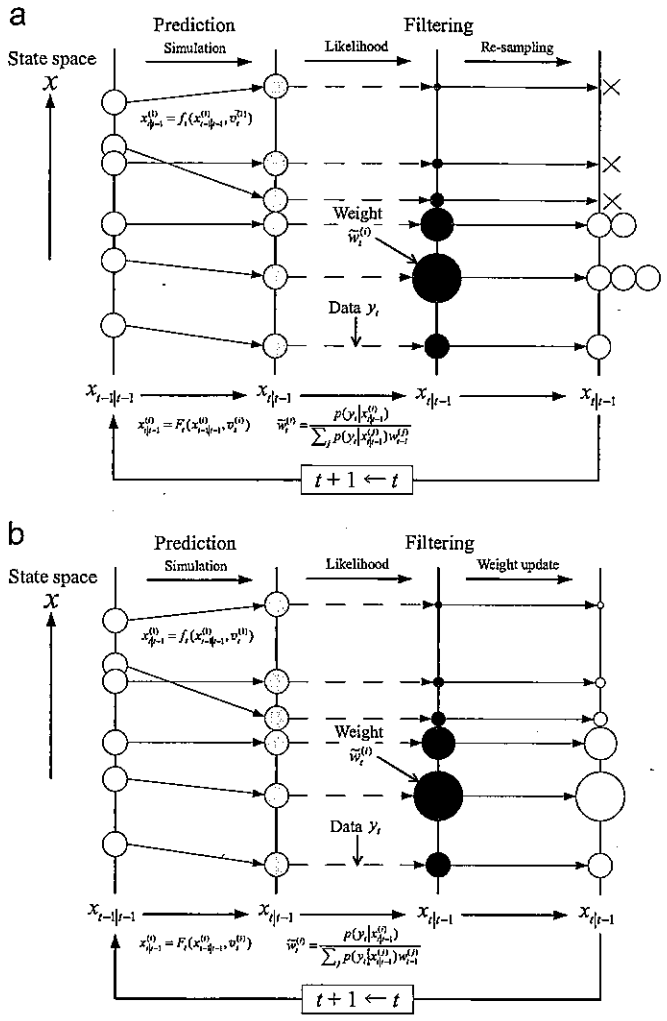

Fig. 6. Algorithms of the PF (modified from Higuchi, 2005). (a) Sampling Importance Resampling (SIR) algorithm and (b) Sequential Importance Sampling (SIS) algorithm.

3. Parameter identification of elasto-plastic materials in numerical tests

3.1. Setup of the numerical test

Fig. 7 presents a schematic illustration of the experiment. The compression-shear behavior of a 20-cm-square clayey soil element was simulated by a finite element analysis, given the incremental load of $\Delta q = 1.0$ kPa/step at every calculation step. The original Cam-clay model was used to describe the elasto-plastic behavior of the soil element which had the material parameters listed in Table 1. In the table, ν, λ, κ, e_0, M, σ'_v, K_0, and OCR are Poisson's ratio, the compression index, the swelling index, the initial void ratio, the critical state parameter, the effective overburden pressure, the coefficient of earth pressure at rest, and the overconsolidation ratio, respectively.

This experiment includes drained and undrained shear tests under monotonous loading. Fig. 8 shows the effective stress paths on the q–p' plane under undrained/drained shear. In this figure, the vertical axis indicates the

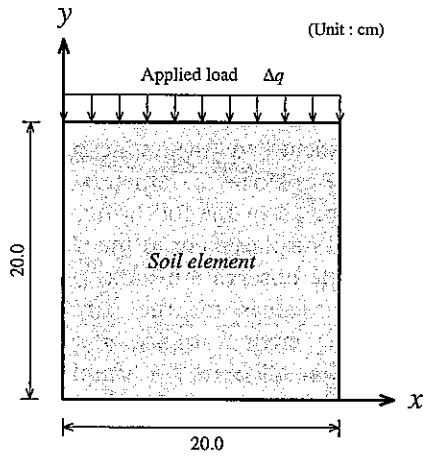

Fig. 7. Schematic illustration of the experiment.

Table 1
Parameters of the soil elements.

ν	λ	κ	e_0	M	$\sigma_{v'}$ (kPa)	K_0	OCR
0.333	0.225	0.083	1.087	1.103	98.0	1.0	1.0

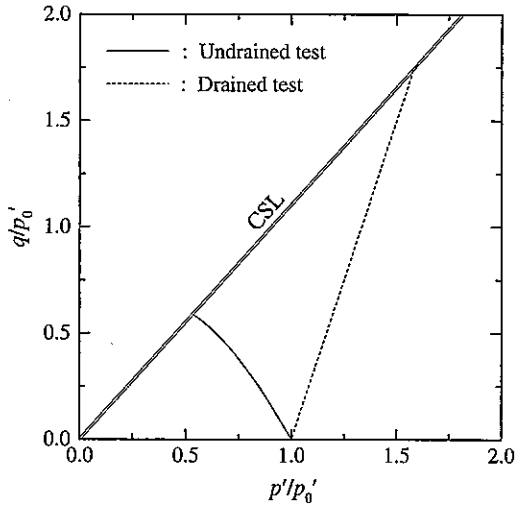

Fig. 8. Effective stress paths of a soil element under undrained/drained shear.

normalized deviatoric stress (q/p'_0) and the horizontal axis indicates the normalized effective mean stress (p'/p'_0). The incremental load of the $\Delta q = 1.0$ kPa/step was applied to the soil elements in both tests until the stress paths reached the critical state line (CSL) . Calculation steps, 120 and 200 in number, were needed for the undrained and drained shear tests, respectively. In the undrained tests, the model boundary was assumed to be impermeable; i.e., no water was able to flow into or out of the element. The total stress path in the drained tests, which is equal to the effective stress path in this case, followed a 1:3 line on the q–p' plane, so that the stress path intersected the CSL at $q/p'_0 = 1.7$.

Fifteen numerical experiments were carried out for both undrained and drained shear tests and the cases are summarized in Table 2. The numerical experiments were assigned a set of conditions, such as the number of parameters to be identified, the number of particles P_n, and error variance σ^2. The parameters to be identified consisted of some or all of the following, namely λ, κ, M, and p'_0. The vertical displacement at the top of the element was used here as the observation data, prepared with the predetermined true values for the parameters listed in Table 3. The same error variance $\sigma^2=0.05$ (cm^2) was assumed and used in all cases for simplicity. The initial ensembles for each parameter were sampled from uniform PDFs, which follow the feasible space listed in Table 4. These values signify the permissible ranges assigned to the parameters to be identified. In Table 2, "O" signifies the target parameters for identification; "-" means the parameters were kept equal to their initial values, which are shown in Table 1.

Table 2
Set of parameters to be identified in undrained/drained shear tests.

Case	Parameters to be identified				P_n	σ^2 (cm^2)
	λ	κ	M	p'_0		
1-1	O	–	–	–	100	0.05
1-2	–	O	–	–	100	
1-3	–	–	O	–	100	
1-4	–	–	–	O	100	
2-1	O	O	–	–	400	
2-2	O	–	O	–	400	
2-3	O	–	–	O	400	
2-4	–	O	O	–	400	
2-5	–	O	–	O	400	
2-6	–	–	O	O	400	
3-1	O	O	O	–	1200	
3-2	O	O	–	O	1200	
3-3	O	–	O	O	1200	
3-4	–	O	O	O	1200	
4-1	O	O	O	O	3600	

Table 3
True values of the parameters to be identified.

Parameter	True value
λ	0.155
κ	0.047
M	1.220
p'_0 (kPa)	74.0

Table 4
Feasible space of the soil parameters to be identified.

Parameter	Feasible space
λ	0.125–0.325
κ	0.033–0.133
M	0.803–1.403
p'_0 (kPa)	68.0–128.0

3.2. Results and discussion

Figs. 9–16 show the time evolution of the identified parameters in the undrained and drained shear tests listed in Table 2. In this paper, the weighted mean values are referred to as "identified parameters," and the values are obtained by

$$\overline{\phi}_t = \sum_{i=1}^{N} w_t^{(i)} \phi_t^{(i)} \tag{16}$$

where $\overline{\phi}_t$ and $\phi_t^{(i)}$ indicate the identified parameter at time step t and parameter of particle number i at time step t, respectively. In these figures, the vertical axis indicates the identified parameters and the horizontal axis indicates the calculation steps. We will use the same legend in Figs. 9–16, where the dotted lines represent the true values and the symbols represent the identified parameters.

The parameter identification of one unknown parameter approaches the true values, although the identification starts, intentionally, with an incorrect $\overline{\phi}_0$ in all cases. These results verify the effectiveness of the PF for the parameter identification of the elasto-plastic model, which presents strong non-linear behavior. The parameter identification of two or three unknown parameters also provided high accuracy; however, identification involving λ as the unknown parameters were less accurate. There are some difficulties in obtaining solutions with high accuracy in the cases of three or four unknown parameters under a given number of particles, observations, and error covariances. The identified parameters at the final step of the assimilation for the undrained and the drained shear tests are listed in Tables 5 and 6, respectively.

Fig. 17 compares the simulated results using the identified parameters of Case 4-1 with the synthetic observation data used for the identification. It is clear that a combination of incorrect parameters can produce almost identical curves. This indicates that a single piece of observation data may lead to the problem of non-uniqueness. In real problems, e.g., embankment constructions on soft grounds, it would be impossible to determine whether the final predicted values for the settlement and the lateral displacement are representative or close to the actual values of the simulated ground. Unlike the finite element simulation, the actual solutions are not known a priori in real construction works. This means, in order for the identification procedure to be useful, the problems with "ill-posedness," particularly, "non-uniqueness," must be improved so that all the parameters to be identified will lead to the true values.

4. Application of the PF to partial loading model tests

4.1. Model test apparatus and procedures

The model test apparatus was manufactured to observe the deformation of a soil block sample loaded partially with constant confining pressure through a rubber

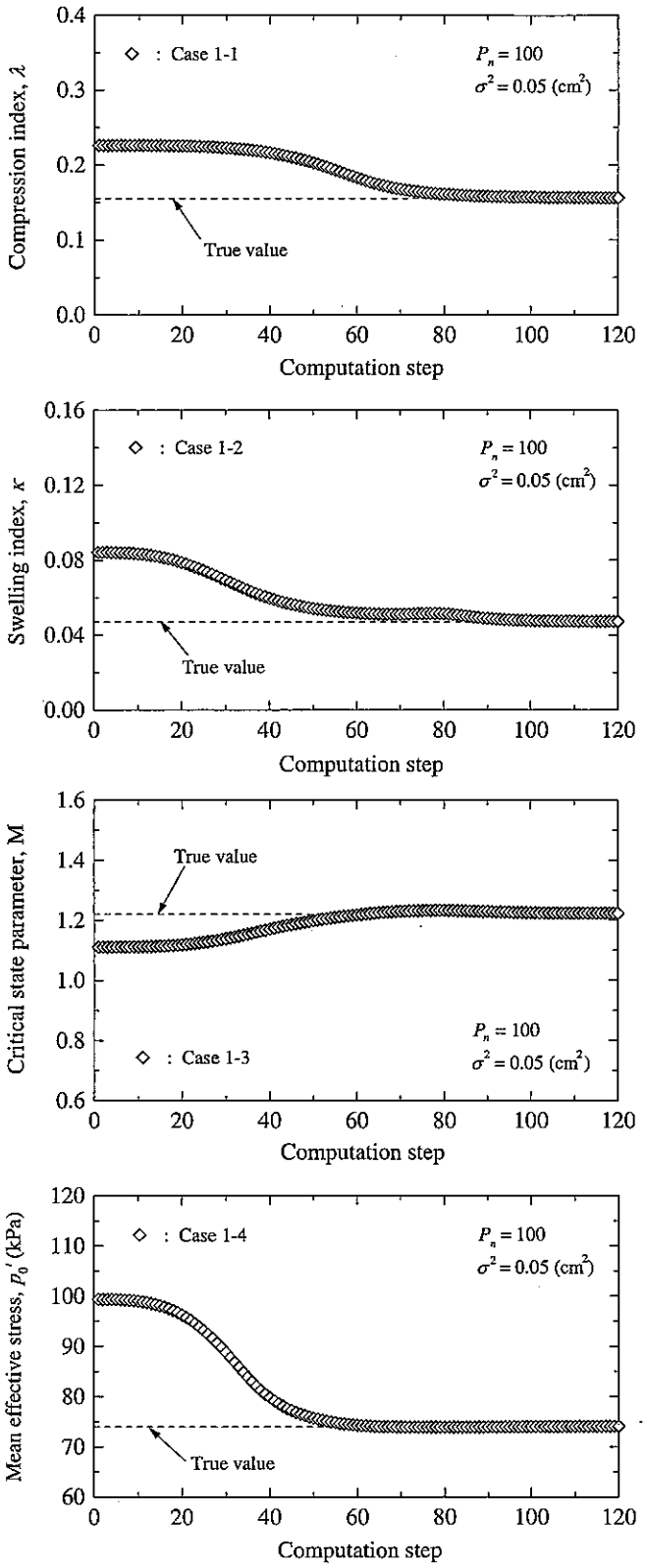

Fig. 9. Parameter identification of one unknown parameter (undrained test, Case 1).

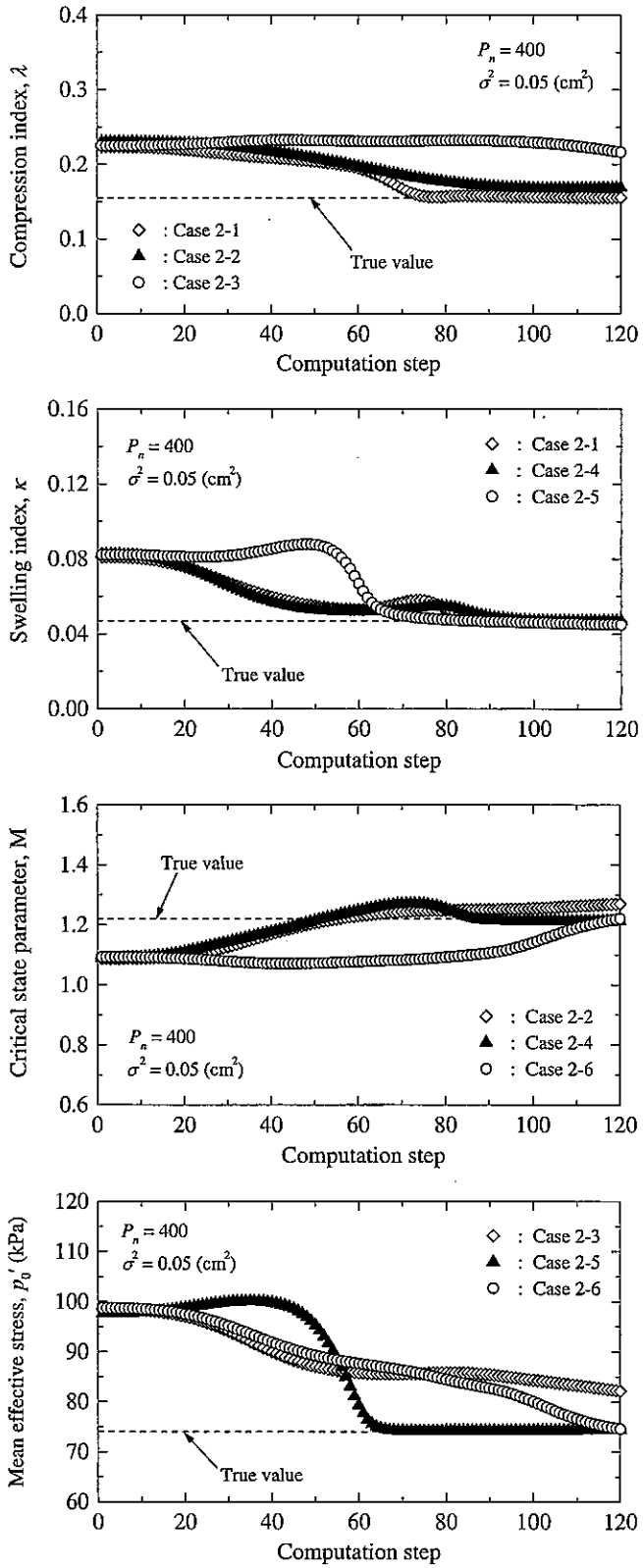

Fig. 10. Parameter identification of two unknown parameters (undrained test, Case 2).

membrane during the tests, as shown in Fig. 18. The apparatus consists of a soil container box, a rigid footing, a loading piston, and several controllers. The front side of the container box was made of transparent acrylic plates to observe the deforming behavior of the soil block. The inside dimensions of the box were as follows: 26 cm in

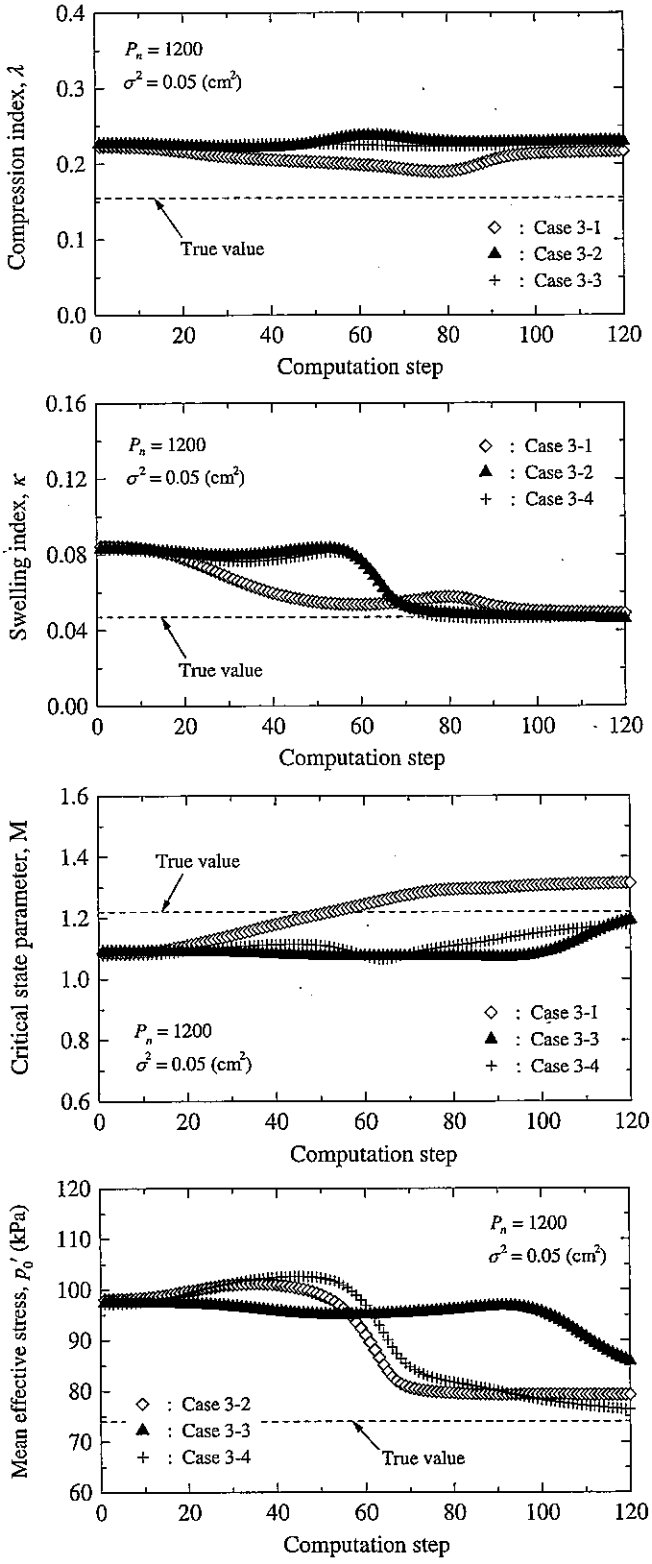

Fig. 11. Parameter identification of three unknown parameters (undrained test, Case 3).

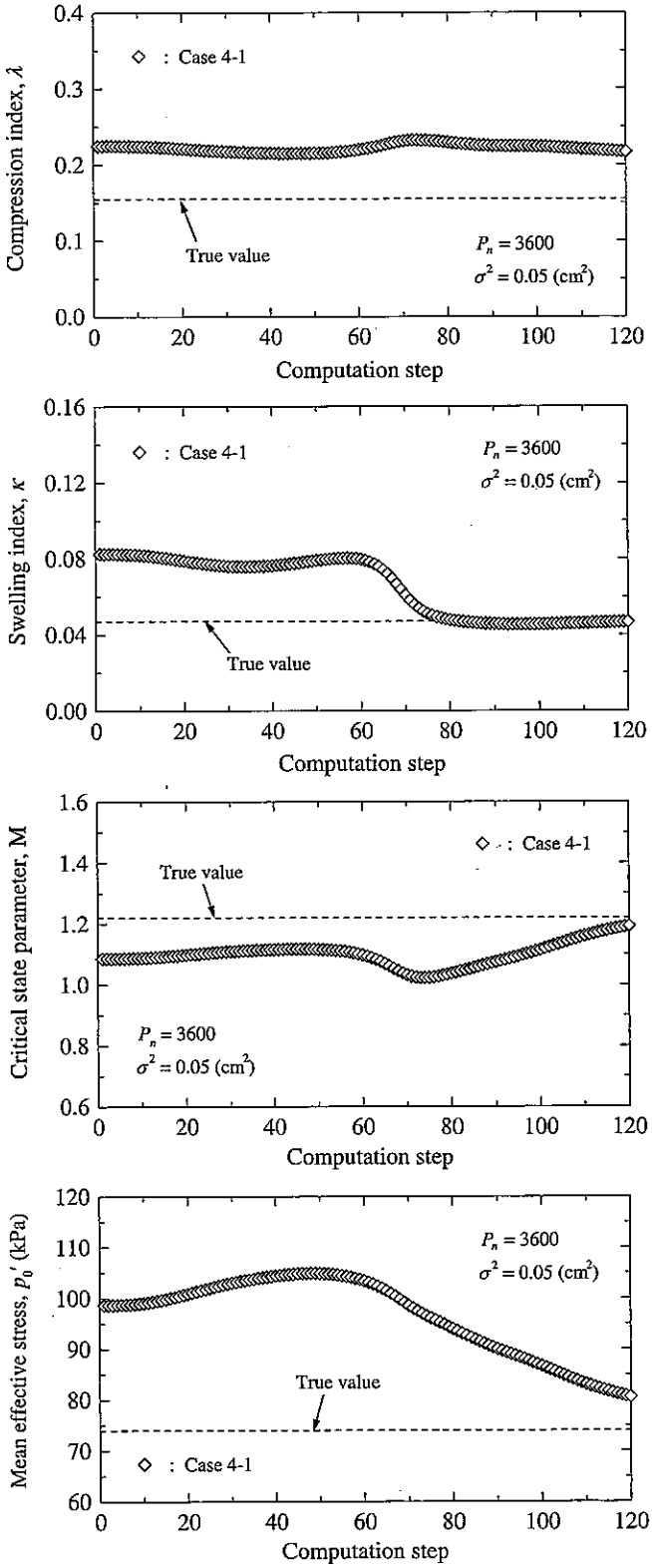

Fig. 12. Parameter identification of four unknown parameters (undrained test, Case 4).

length, 10 cm in width, and 9.5 cm in height. In order to minimize the wall friction, the surface inside the box was lubricated with silicone oil.

The soil sample was prepared from commercially available kaolin clay, which has been used extensively in geotechnical model tests, and whose physical properties

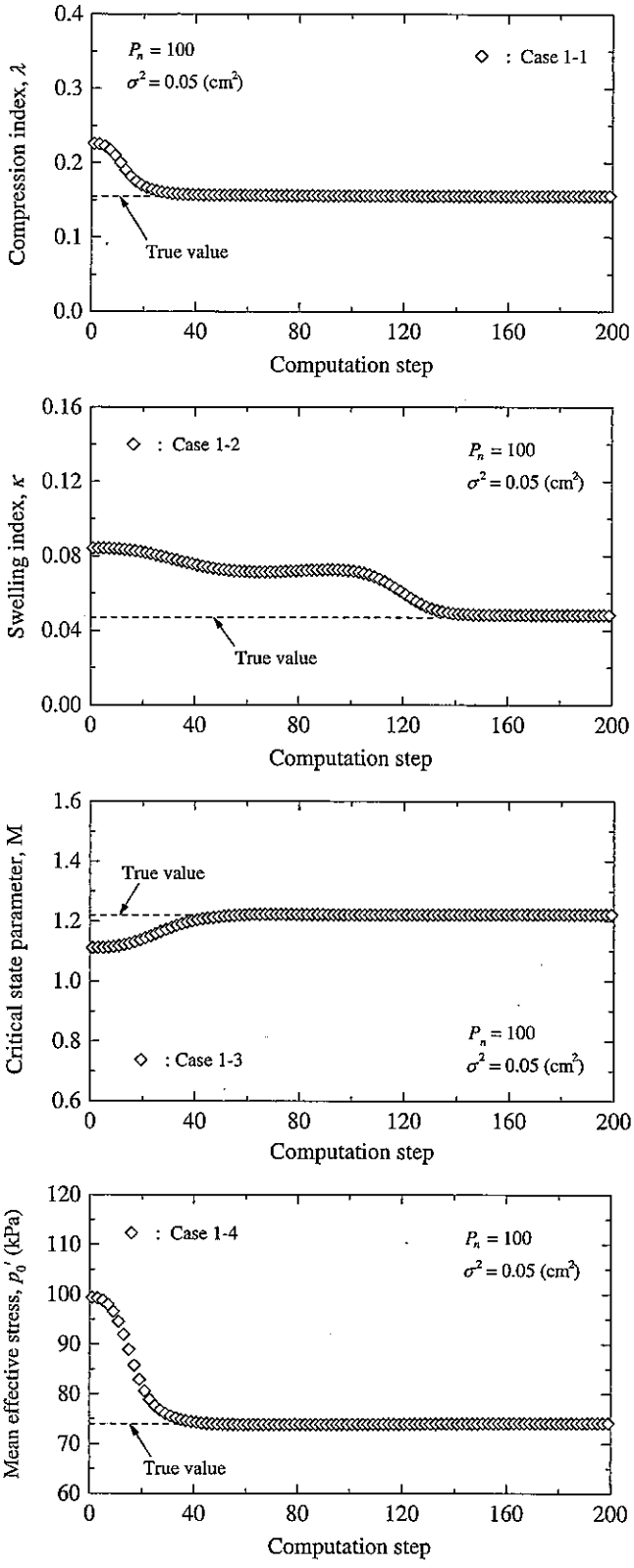

Fig. 13. Parameter identification of one unknown parameter (drained test, Case 1).

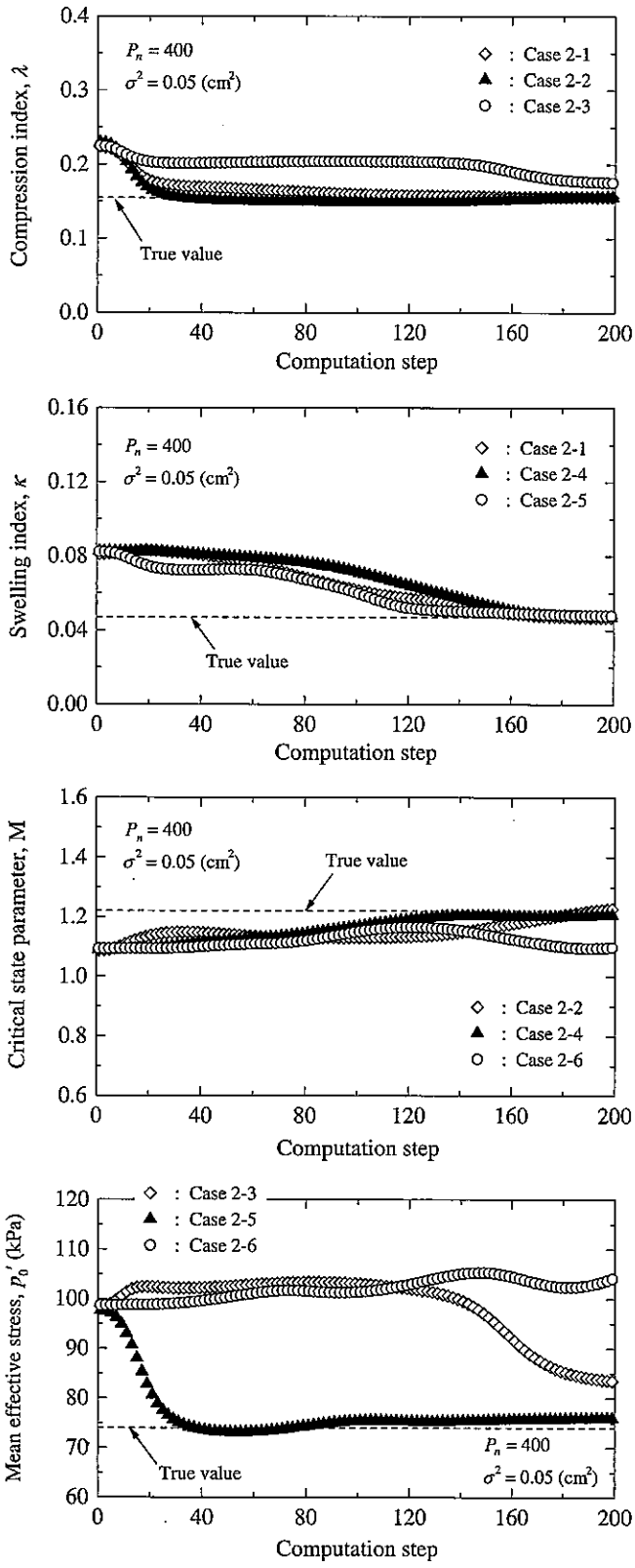

Fig. 14. Parameter identification of two unknown parameters (drained test, Case 2).

are shown in Table 7. In the table, ρ_s, w_I, w_L, w_P, and I_p signify the density of the soil particles, the initial water content, the liquid limit, the plastic limit, and the plasticity index. The soil block sample was made at a preliminary consolidation pressure of 49 kPa. Firstly, a confining pressure of 147 kPa was furnished by a back pressure of

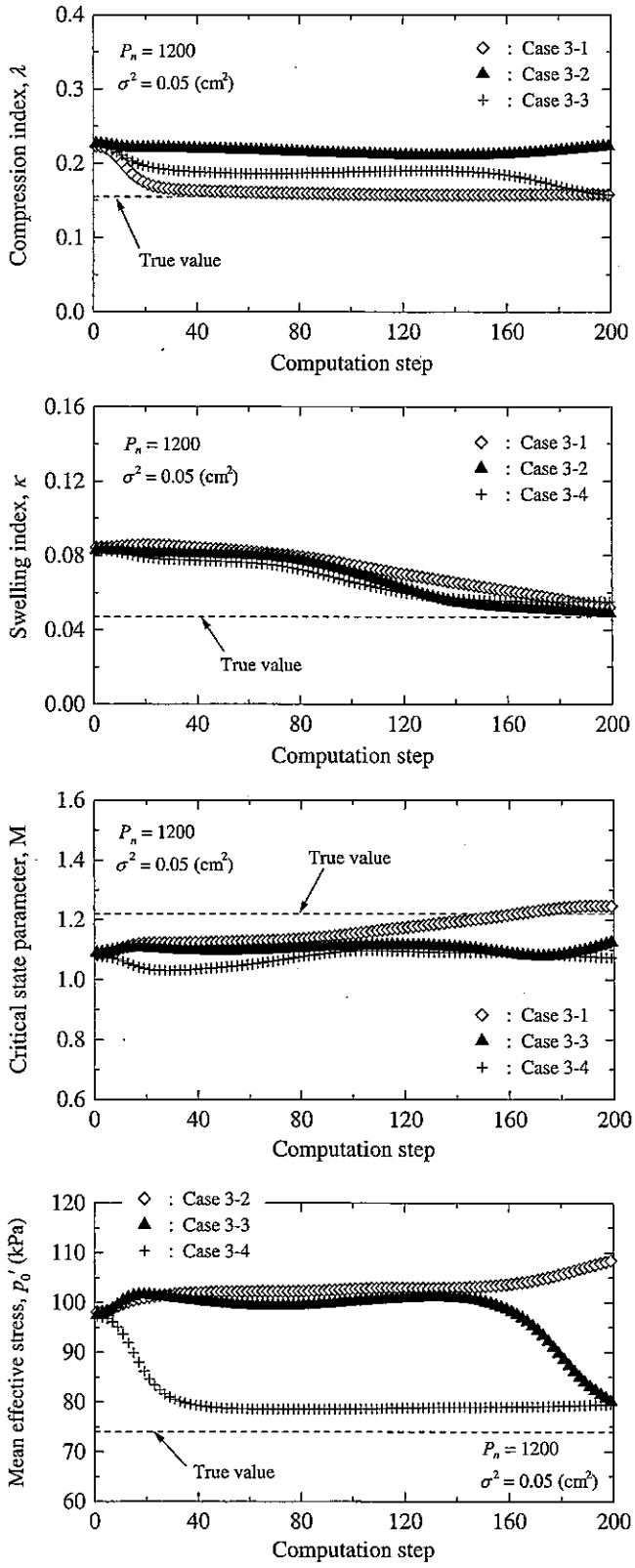

Fig. 15. Parameter identification of three unknown parameters (drained test, Case 3).

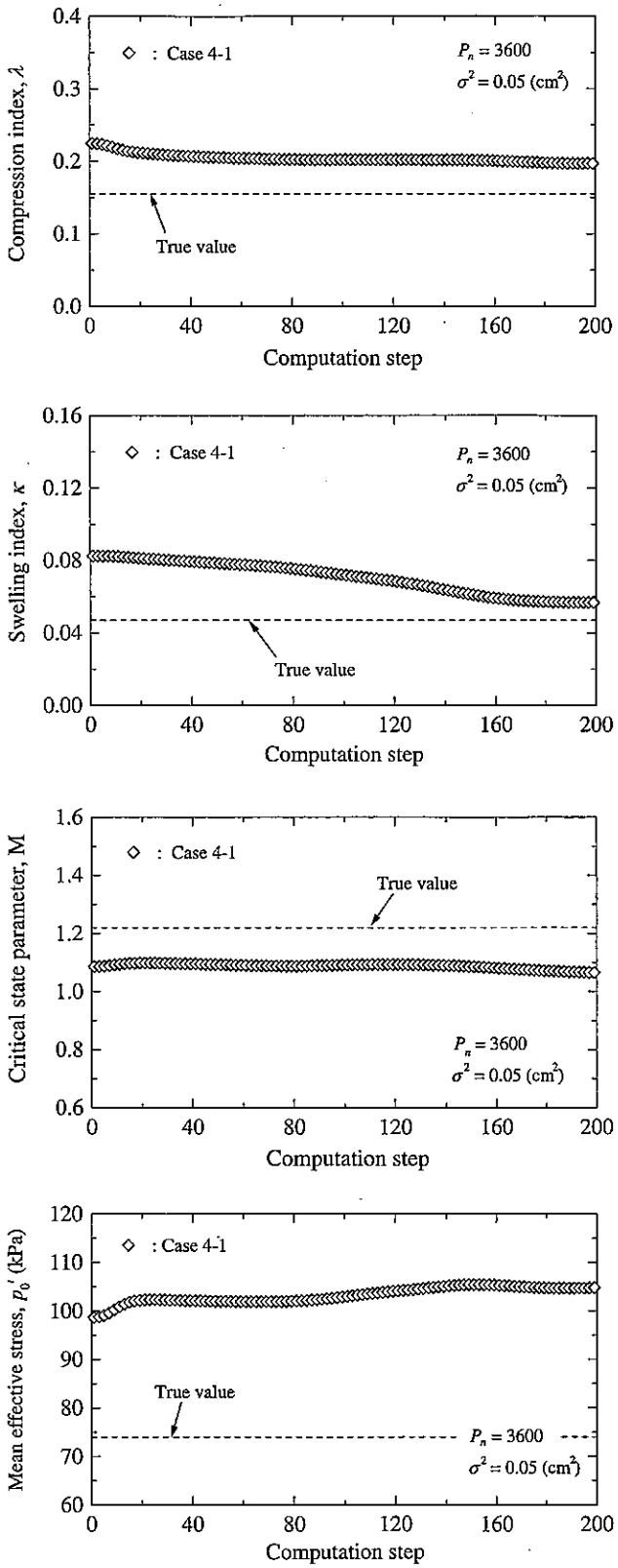

Fig. 16. Parameter identification of four unknown parameters (drained test, Case 4).

98 kPa. After one-dimensional consolidation with a consolidation pressure of 49 kPa (=147−98 kPa), a total partial load of 88.2 kPa was applied to the right side of the soil block, as shown in Fig. 18. Fig. 19 shows the loading history used in these tests. Fig. 20 shows the placement of the measurement instruments, which include

Table 5
Parameter values finally identified in undrained shear tests.

Case	Identified parameters			
	λ	κ	M	p'_0
True value	0.155	0.047	1.220	74.0
1-1	0.156	–	–	–
1-2	–	0.047	–	–
1-3	–	–	1.223	–
1-4	–	–	–	74.1
2-1	0.156	0.047	–	–
2-2	0.169	–	1.270	–
2-3	0.216	–	–	82.2
2-4	–	0.047	1.213	–
2-5	–	0.045	–	74.4
2-6	–	–	1.220	74.6
3-1	0.217	0.049	1.313	–
3-2	0.230	0.046	–	79.2
3-3	0.227	–	1.193	85.8
3-4	–	0.047	1.179	76.3
4-1	0.217	0.047	1.192	80.6

Table 6
Parameter values finally identified in drained shear tests.

Case	Identified parameters			
	λ	κ	M	p'_0
True value	0.155	0.047	1.220	74.0
1-1	0.156	–	–	–
1-2	–	0.048	–	–
1-3	–	–	1.222	–
1-4	–	–	–	74.1
2-1	0.156	0.047	–	–
2-2	0.156	–	1.228	–
2-3	0.176	–	–	83.5
2-4	–	0.047	1.201	–
2-5	–	0.048	–	76.0
2-6	–	–	1.099	104.3
3-1	0.158	0.052	1.246	–
3-2	0.223	0.049	–	108.5
3-3	0.157	–	1.129	79.8
3-4	–	0.055	1.073	79.5
4-1	0.197	0.057	1.064	104.7

displacement-tracing pointers (A–F) and pressure transducers (P1–P3). Since the front of the apparatus was made of transparent acrylic plates, the movements of the pointers during the test were able to be recorded with a digital video camera. The pore pressure was continuously measured until the excess pore pressure had completely dissipated.

4.2. Simulation and setup of DA

The two-dimensional behavior of the block sample was predicted by a soil–water coupled finite element analysis with the Cam-clay model. Fig. 21 shows the finite element mesh and the boundary conditions used for this analysis.

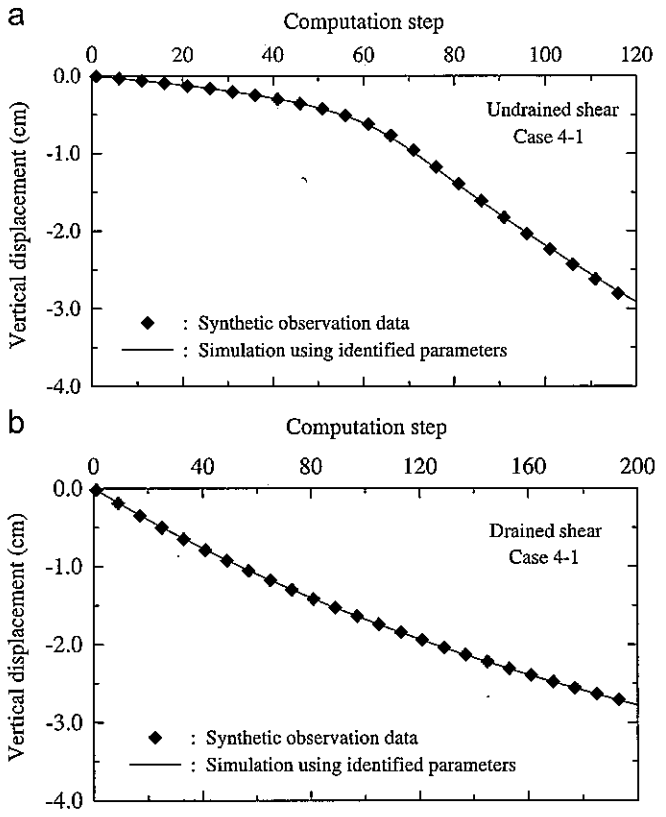

Fig. 17. Illustration of non-uniqueness problem in parameter identification. (a) Undrained shear test and (b) drained shear test.

The loading plate was assumed to be linear elastic and represented by a single column of elements with sufficient stiffness. The values of the Cam-clay parameters and the permeability of the block sample, estimated on the basis of plasticity index I_p, are listed in Table 8. The values in the parentheses represent the initial values for parameter identification. The determination of the input parameters followed the procedures proposed by Iizuka and Ohta (1987) and Nakase et al. (1988) for elasto-plastic/elasto-viscoplastic constitutive models, which are summarized in Table 9.

The application example in this chapter identified the compression index λ, the critical state parameter M, and the coefficient of permeability k, since these three parameters were found to be sensitive in the calculation. Just at the time of partial loading, the clay block presented undrained behavior, which is governed by strength parameters such as effective internal friction angle ϕ'. On the other hand, after the loading process, the block exhibits consolidation behavior, which is influenced by consolidation parameters, such as λ and k. Since the number of parameters should be reduced for this parameter identification, the swelling index κ and the void ratio e_0 were given after being estimated from plasticity index I_p. In this problem, 1200 sets of particles, which were generated as uniform random numbers, were utilized. Table 10 shows the feasible ranges of the parameters to be identified.

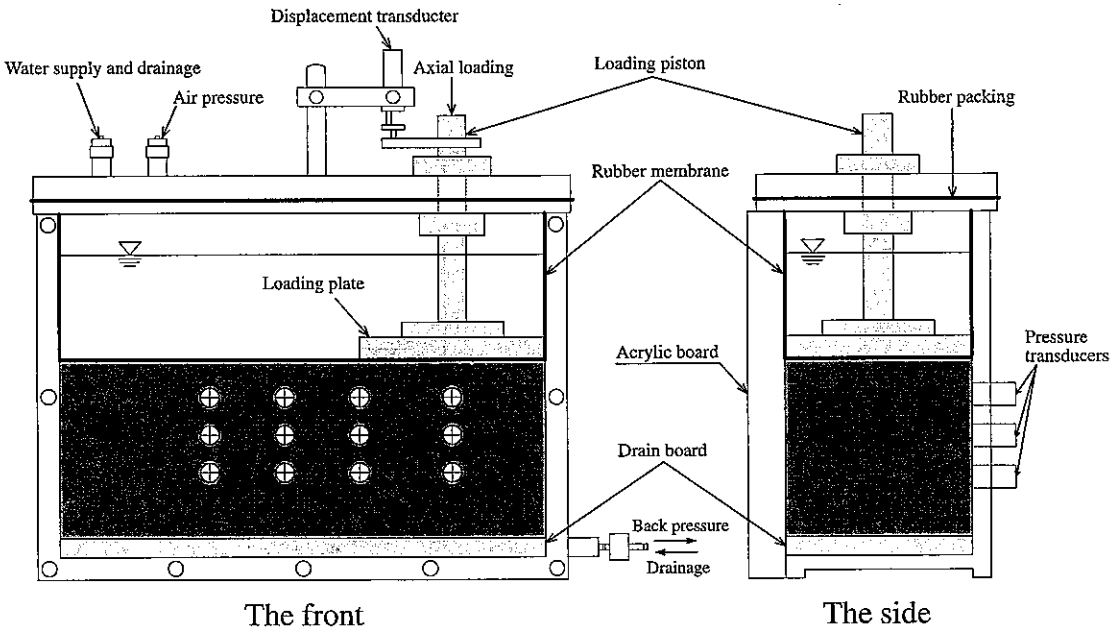

Fig. 18. Model test apparatus.

Table 7
Physical properties of Kaolin clay.

ρ_s (g/cm^3)	w_I (%)	w_L (%)	w_P (%)	I_p (%)	Clay fraction (%)	Silt fraction (%)
2.63	52.9	58.2	37.4	20.8	42	58

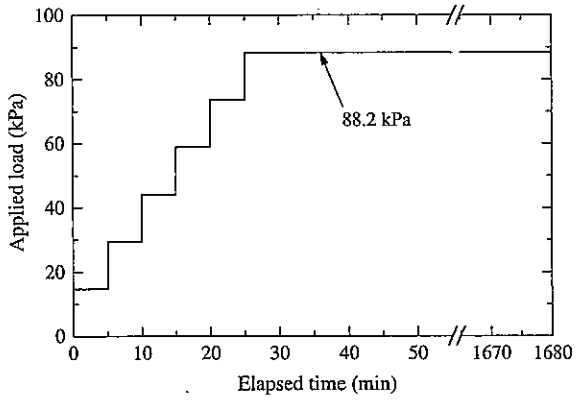

Fig. 19. Loading process of the model test.

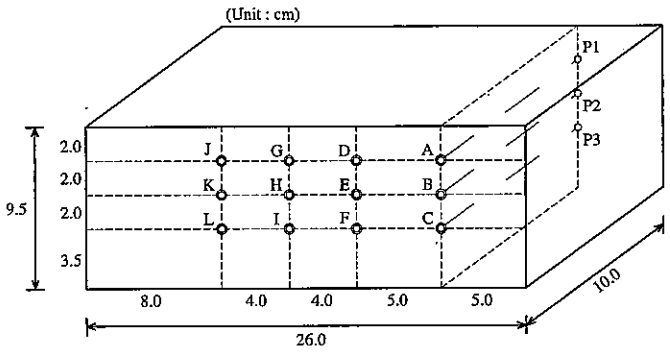

Fig. 20. Block sample size and placement of measurement instruments.

Although the settlement and the lateral displacement, measured at twelve points (A–L), and the pore water pressure, measured by three transducers (P1–P3), as shown in Fig. 21, were available, the settlement measured at pointers A, B, and C and the lateral displacement measured at pointers D, E, and F were used for this analysis. This is because these measurement data just beneath the loading plate are more responsive to the applied load than the other data.

In case of using different types of observation data that do not have the same units, such as displacements and pore pressures, additional considerations are required. This is because observed displacements and pore pressures usually have a different order of magnitude of values and levels of error, and can have different effects on the DA results. In fact, the measured pore pressure values include relatively large observation errors even though the displacements are measured with higher accuracy. A strategy to overcome the above issues includes the incorporation of a scaling parameter into Eq. (14). The scaling parameter controls

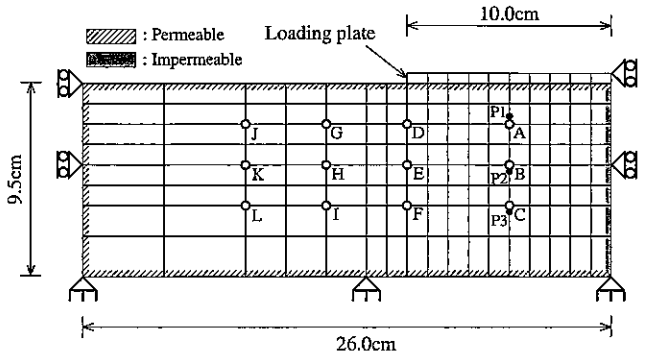

Fig. 21. Finite element mesh and the boundary conditions.

Table 8
Parameter values of the soil block sample.

ν	λ	κ	e_0	M	k (cm/min)
0.333	(0.114)	0.014	0.912	(1.209)	(1.0×10^{-9})

Table 9
Simplified determination procedure for soil parameters based on the I_p.

$\lambda=0.015+0.007I_p$	Iizuka and Ohta (1987)
$\sin\phi'=0.81-0.233\log(I_p)$	
$M=6\sin\phi'/(3-\sin\phi')$	
$\kappa=M/(1.75\lambda)-1$	
$e=0.517+0.019I_p$	Nakase et al. (1988)

Table 10
Feasible parameter space for parameters to be identified.

Parameters to be identified	Feasible parameter space
λ	0.08–0.38
M	0.90–1.50
k (cm/min)	1.0×10^{-3}–1.0×10^{-8}

the effect between measured displacements and pore pressure, and its value can be appropriately determined using model selection techniques, e.g., Akaike Bayesian Information Criterion (ABIC; Akaike, 1980) and cross-validation (e.g., Bishop, 2006).

It is an important task to determine covariance matrix R_t. In this analysis, a statistical method for evaluating and comparing models referred to as the holdout validation was utilized to determine covariance matrix R_t (e.g., Kohavi, 1995). This method splits the observation data into two mutually exclusive subsets: a training set and a holdout set. In this method, a model is fit to the training data, and the accuracy of the predictions is assessed using the holdout set. The holdout validation appropriated in this analysis is summarized in Appendix A.

Assuming that all observation errors are independent of each other, covariance matrix R_t is presented as follows:

$$R_t=\begin{bmatrix} 0.05100 & 0.00000 & 0.00000 & 0.00000 & 0.00000 & 0.00000 \\ 0.00000 & 0.02520 & 0.00000 & 0.00000 & 0.00000 & 0.00000 \\ 0.00000 & 0.00000 & 0.00960 & 0.00000 & 0.00000 & 0.00000 \\ 0.00000 & 0.00000 & 0.00000 & 0.00780 & 0.00000 & 0.00000 \\ 0.00000 & 0.00000 & 0.00000 & 0.00000 & 0.01200 & 0.00000 \\ 0.00000 & 0.00000 & 0.00000 & 0.00000 & 0.00000 & 0.00090 \end{bmatrix} \quad (17)$$

where the non-diagonal covariance terms were assumed to be zero.

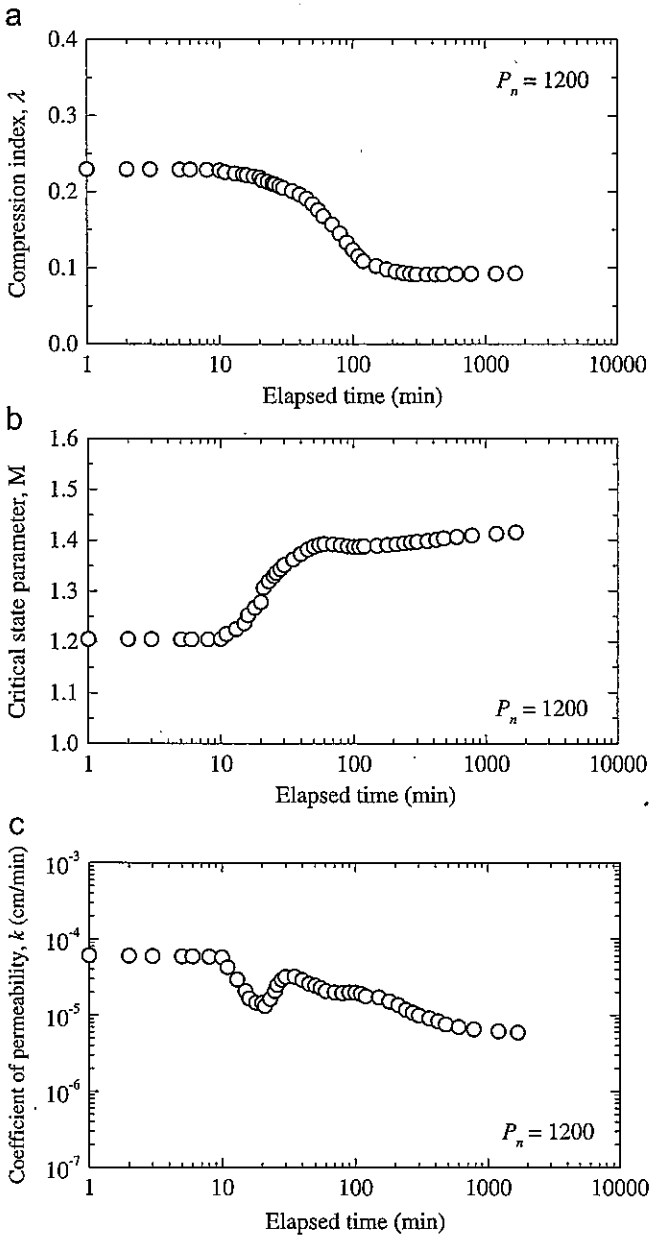

Fig. 22. Time evolution of identified parameters. (a) Compression index, λ (b) critical state parameter, M and (c) coefficient of permeability, k.

4.3. Results and discussion

Fig. 22 shows the time evolution of the identified parameters, and (a), (b), and (c) in the figure are the results of compression index λ, critical state parameter M, and coefficient of permeability k, respectively. The assimilation starts with the weighted mean values of the particles prepared at the initial stage, i.e., $\lambda=0.22927$, $M=1.20546$, and $k=6.095\times10^{-6}$ (cm/s). At the beginning of the tests (1–10 min), each identified parameter stays almost constant. However, after a lapse of 10 min or more, each parameter changes dramatically. By the end of the test, each value has become nearly constant again. After a lapse of 1680 min, the identified parameters are as follows:

$$\lambda=0.092684,\quad M=1.415355,\quad \text{and}\quad k=5.90975510^{-6}\ (\text{cm/s}) \tag{18}$$

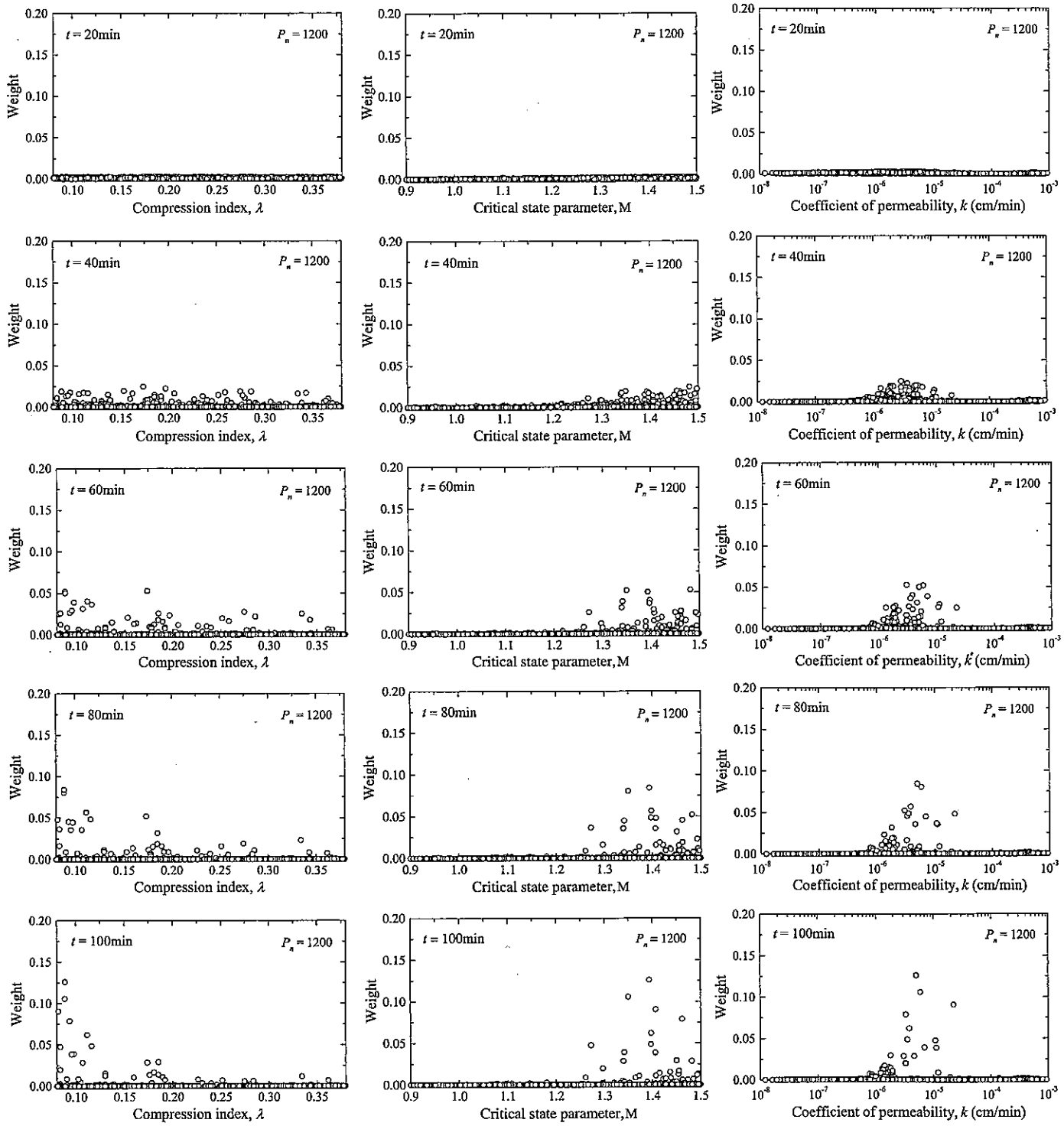

Fig. 23. Filtered distribution of weight.

Fig. 23 shows the filtered distributions of the weights for compression index λ, critical state parameter M, and coefficient of permeability k. In these figures, the vertical axis is the weight and the horizontal axis is the parameter value. According to these figures, after a lapse of 20 min, most of the weights were uniformly distributed. After a lapse of 40 min, however, some particles had gained a significant amount of weight. After a lapse of 60 min, the weights of only a few specific particles had become higher. The distribution at a lapse of 100 min had a smaller variance than the distribution at a lapse of 20 min; therefore, the uncertainties about the identified parameters had decreased. We see that, unlike the Gaussian filter e.g., the KF, the arbitrary PDFs can be evaluated using a large number of particles. This is the remarkable advantage of the PF.

The three identified parameters, i.e., λ, M, and k, were used to simulate the time-settlement and the time-lateral displacement relationships of the soil block. Figs. 24 and 25 compare the simulation results using the identified parameters with the settlement measured at A, B, and C and the lateral displacements at D, E, and F. In these figures, four lines, namely DA (20 min), DA (60 min), DA (100 min), and DA (1680 min), signify the simulation results obtained by the parameters identified up to 20, 60, 100, and 1680 min, respectively. In Fig. 24, the simulation results using parameters identified at the beginning of the experiment, DA (20 min) and DA (40 min),

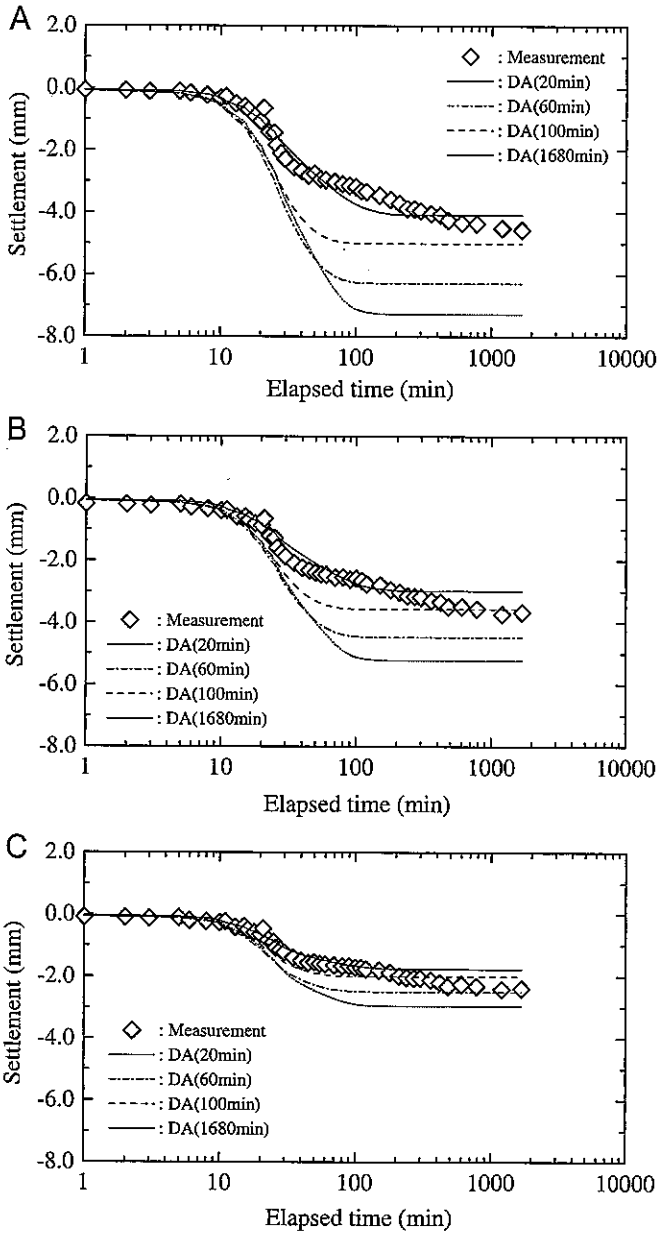

Fig. 24. Simulation results of time-settlement relationship using the identified parameters.

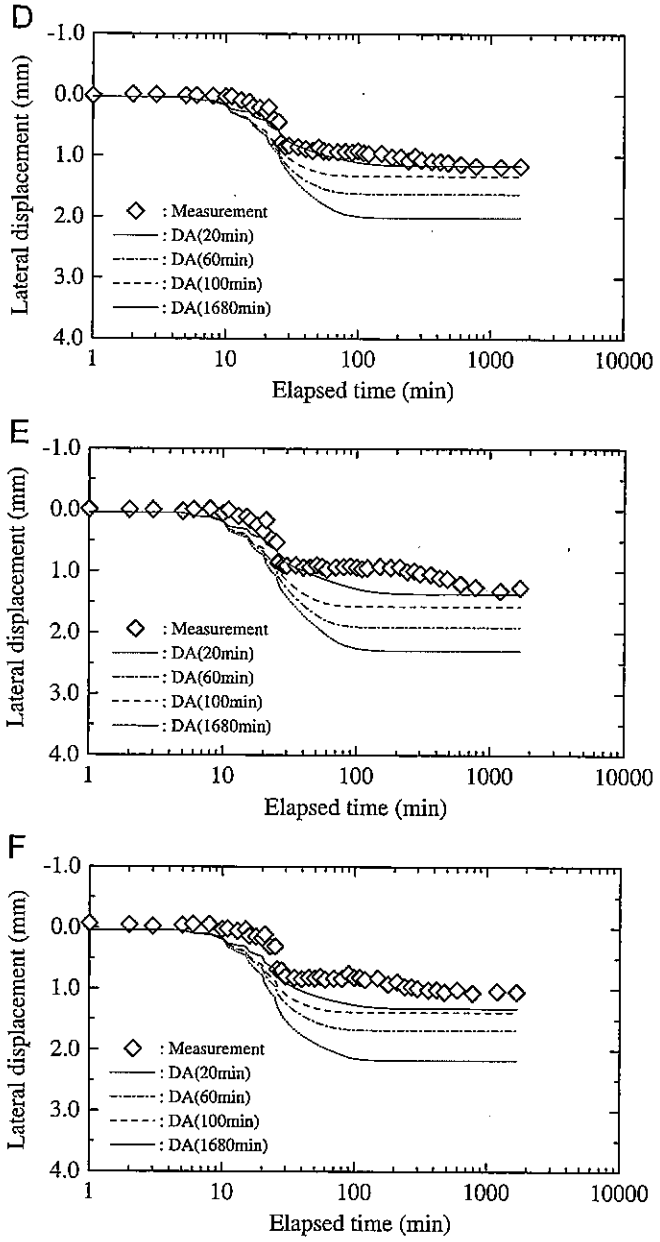

Fig. 25. Simulation results of time-lateral displacement relationship using identified parameters.

deviate somewhat from the measurements. However, the results for DA (100 min) and DA (1680 min) show a good agreement with the measured values. Similar results to those for the lateral displacements (Fig. 25) were observed. It is remarkable that long-term predictions can be achieved with high accuracy, even though we used only the measured data for 100 min.

5. Concluding remarks

This study has investigated the theoretical and the practical effectiveness of the DA method, i.e., the PF, for geotechnical problems, by applying the methodology to the numerical experiments and the model test. First, we have outlined the concepts and methods of DA, and the PF, which has high potential for application to geotechnical engineering, was addressed and its mathematical formulation and algorithms were briefly reviewed. Then, we have dealt with the numerical experiments for the shear behavior of a soil element under undrained/drained conditions, where the model parameters of elasto-plastic model have been identified by the PF. Finally, the PF has been applied to the actual model test and the validity was evaluated by a comparison between the filtering performance and the corresponding experimental data. The following remarks can be noted:

(1) The PF does not require assumptions of linearity or Gaussianity; it is applicable to general problems. In addition, the PF method uses the recursive formula of the sequential Bayesian framework directly and approximates the posterior probability distributions by means of appropriate weights associated with each realization. The sampling methods of the PF can be split into the SIR and the SIS. Since the mechanical behavior of soils depends on both the current stress and the recent stress history of the soil, the SIS algorithm performs better in geotechnical problems than the SIR algorithm. Thus, it has been confirmed that the PF with the SIS algorithm holds the greatest potential for application to geotechnical engineering, and that existing technical problems in geomechanics can be overcome through its use.
(2) The numerical tests have shown that the parameters identified by the PF have converged into their true values, and the approach presented in this study has shown great promise as an accurate parameter-identification method for elasto-plastic geomaterials.
(3) The simulation results using the identified parameters obtained with the PF were close to the actual measurement data, and long-term predictions with high accuracy were able to be achieved even though short-term measurement data were used. The PF approach produces more information about the parameters of interest than simple estimated values obtained from a variational DA method; namely, the identification comes in the form of a PDF. The usefulness of the PF approach for geotechnical practices was presented through these results.

Appendix A

Here, we briefly show the holdout validation which was used to determine covariance matrix R_t. The holdout validation is a statistical method for evaluating and comparing simulation models; it splits the data into two mutually exclusive subsets, called a training set and a holdout set or testing set, to avoid any overlap between the training data. In this method, for each split, a model is fit to the training data and the accuracy of the prediction is assessed using the holdout set. In order to estimate the accuracy of the models, a k-fold cross-validation is often utilized. Although the k-fold cross-validation is a powerful method for variable selection, a large-scale (high dimensional) cross-validation is complicated and computationally expensive. Therefore, a holdout validation was utilized from the viewpoint of a simplicity and computation costs.

Firstly, we suppose that covariance matrix R_t can be written by the following formula:

$$R_t^{(i)} = \alpha^{(i)}\beta_j\delta_{jk} = \begin{bmatrix} \alpha^{(i)}\beta_1 & 0 & \cdots & 0 \\ 0 & \alpha^{(i)}\beta_2 & \cdots & \vdots \\ \vdots & \vdots & \ddots & 0 \\ 0 & \cdots & 0 & \alpha^{(i)}\beta_n \end{bmatrix} \quad (i=1,2,...,m, j=1,2,...,n) \tag{A1}$$

where $\alpha^{(i)}$, β_j, and δ_{jk} are the fitting parameter, the error variance, and Kronecker's delta, respectively. Superscript (i) is the number of fitting parameters, and subscript j is the observation point number. Then, non-diagonal covariance term $R_t^{(i)}$ is assumed to be zero for simplicity. The following paragraph notes the details of the determination flow.

A.1. Data partitioning

In a holdout validation, the observation data are split into a training data set and a holdout set. Here, we designated 3/4 of the observation data as the training set and the remaining 1/4 as the holdout set. Fig. A1 shows the processed data at observation point A.

A.2. Error variance β_j

The error variance β_j is determined in terms of predicted displacements u_j $(j=1,2...,n)$ at each displacement point by

$$\beta_j = \left(\frac{u_j}{\sum_{j=1}^{n}|u_j|}\right)^2 = \left(\frac{u_j}{|u_1|+|u_2|+\cdots+|u_n|}\right)^2 \tag{A2}$$

where n is the number of observation points and $|\cdot|$ stands for the absolute values. The values for u_j were obtained from the simulation using the predetermined soil parameters listed in Table 8, and they are shown in Fig. A2.

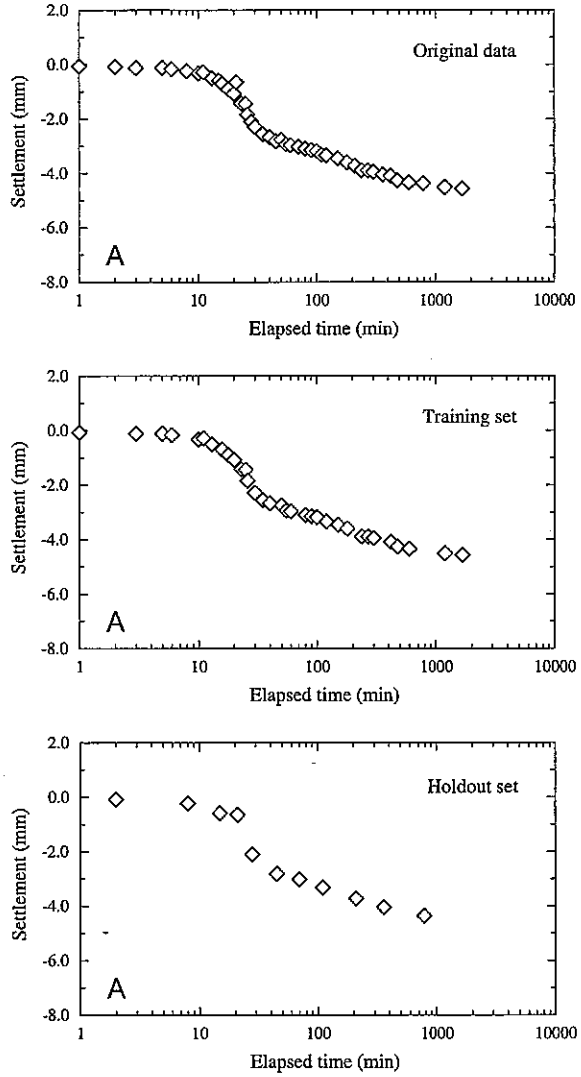

Fig. A1. Training and holdout set.

In these figures, u_j stands for the displacements at each displacement marker at the end of the observation term. Therefore, $j=1,2,\ldots,6$ corresponds to $j=$A, B,…,F.

Calculating β_j for each displacement pointer, and incorporating Eq. (A2) into Eq. (A1), yields the following formula:

$$R_t^{(i)} = \begin{bmatrix} 0.085\alpha^{(i)} & 0 & 0 & 0 & 0 & 0 \\ 0 & 0.042\alpha^{(i)} & 0 & 0 & 0 & 0 \\ 0 & 0 & 0.016\alpha^{(i)} & 0 & 0 & 0 \\ 0 & 0 & 0 & 0.013\alpha^{(i)} & 0 & 0 \\ 0 & 0 & 0 & 0 & 0.020\alpha^{(i)} & 0 \\ 0 & 0 & 0 & 0 & 0 & 0.015\alpha^{(i)} \end{bmatrix} \quad \text{(A3)}$$

A.3. Fitting parameter $\alpha^{(i)}$

Parameters $\alpha^{(i)}$ $(i=1, 2,\ldots,m)$ are scholarly values, which adjust covariance matrix $R_t^{(i)}$. Several values are assumed as $\alpha^{(i)}$ and the optimum value is selected using the holdout validation. Here, the 21 values are set as $\alpha^{(i)}$, which are

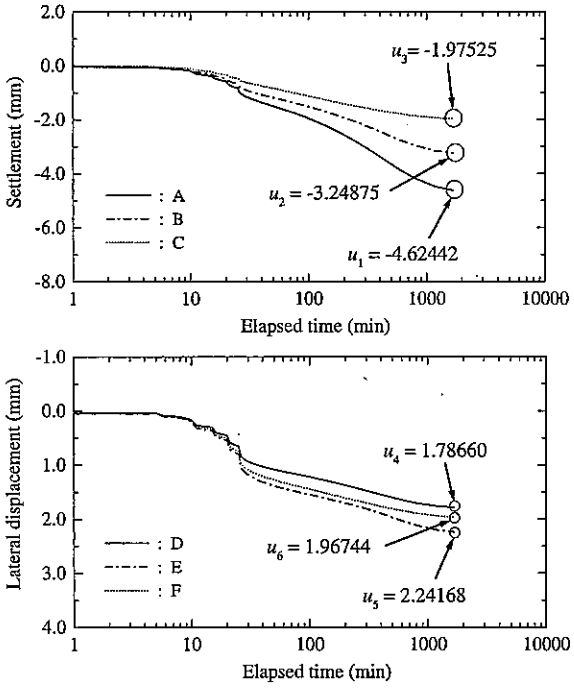

Fig. A2. The prior predicted results of the displacements.

0.001, 0.002, 0.004, 0.006, 0.008, 0.01, 0.02, 0.04, 0.06, 0.08, 0.1, 0.2, 0.4, 0.6, 0.8, 1.0, 2.0, 4.0, 6.0, 8.0, and 10.0.

A.4. Objective function

The $\alpha^{(i)}$, which minimizes objective function $J^{(i)}$ given by Eq. (A4), is adopted as the optimum fitting parameter

$$J^{(i)} = \sum_{j=1}^{n} \left\{ \frac{\sum_{t=1}^{NT} (u_{n,t}^{(i)} - \overline{u}_{n,t})^2}{\sum_{i=1}^{m} (\sum_{t=1}^{NT} (u_{n,t}^{(i)} - \overline{u}_{n,t})^2)} \right\} \quad \text{(A4)}$$

where t is the time step of the testing set and NT is the number of plots of testing data. The $u_{n,t}^{(i)}$ and $\overline{u}_{n,t}$ are the simulated and the measured displacements of measurement point i at time step t for each $\alpha^{(i)}$.

As a result, $\alpha^{(i)} = 0.6$ produced the minimum $J^{(i)}$ and the optimum covariance matrix R_t is given as

$$R_t = \begin{bmatrix} 0.05100 & 0.00000 & 0.00000 & 0.00000 & 0.00000 & 0.00000 \\ 0.00000 & 0.02520 & 0.00000 & 0.00000 & 0.00000 & 0.00000 \\ 0.00000 & 0.00000 & 0.00960 & 0.00000 & 0.00000 & 0.00000 \\ 0.00000 & 0.00000 & 0.00000 & 0.00780 & 0.00000 & 0.00000 \\ 0.00000 & 0.00000 & 0.00000 & 0.00000 & 0.01200 & 0.00000 \\ 0.00000 & 0.00000 & 0.00000 & 0.00000 & 0.00000 & 0.00090 \end{bmatrix} \quad \text{(A5)}$$

References

Akaike, H., 1980. Likelihood and Bayes procedure with discussion. In: Bernado, J.M., DeGroot, M.H., Lindley, D.V., Smith, A.F.M. (Eds.), Bayesian Statistics, vol. 143–166. Valencia University Press, pp. 185–203.

Arai, K., Ohta, H., Kojima, K., 1984. Estimation of soil parameters based on monitored movement of subsoil under consolidation. Soils and Foundations 24 (4), 95–108.

Arai, K., Ohta, H., Kojima, K., Wakasugi, M., 1986. Application of back-analysis to several test embankments on clay deposits. Soils and Foundations 26 (2), 60–72.

Arai, K., Ohta, H., Kojima, K., 1987. Estimation of nonlinear constitutive parameters based on monitored movement of subsoil under consolidation. Soils and Foundations 27 (1), 35–49.

Asaoka, A., 1978. Observational procedure of settlement prediction. Soils and Foundations 18 (4), 87–101.

Asaoka, A., Noda, T., Yamada, E., Kaneda, K., Nakano, M., 2002. An elasto-plastic description of two distinct volume change mechanisms of soils. Soils and Foundations 42 (5), 47–57.

Atkinson, J.H., Richardson, D., Stallebrass, S.E., 1990. Effect of recent stress history on the stiffness of overconsolidated soil. Géotechnique 40 (4), 531–540.

Awaji, T., Masafumi, K., Ikeda, M., Ishikawa, Y., 2009. Data Assimilation. Kyoto University Press in Japanese.

Bennett, A.F., 1992. Inverse Methods in Physical Oceanography. Cambridge University Press.

Bennett, A.F., 2002. Inverse Modeling of the Ocean and Atmosphere. Cambridge University Press.

Bishop, C.M., 2006. Pattern Recognition and Machine Learning. Springer.

Brand, E.W. and Premchitt, J. 1989: Comparison of the predicted and observed performance of the Muar test embankment. In: Proceedings of the International Symposium on Trial Embankments on Malaysian Marine Clays, Kuala Lumpur, 2, pp. 10.1–10.29.

Doucet, A., Godsill, S., Andrieu, C., 2000. On sequential Monte Carlo sampling methods for Bayesian filtering. Statistics and Computing 10, 197–208.

Evensen, G., 1994. Sequential data assimilation with a non-linear quasi-geostrophic model using Monte Carlo methods to forecast error statistics. Journal of Geophysical Research 99, 10143–10162.

Finno, R.J., Calvello, M., 2005. Supported excavations: observational method and inverse modeling. Journal of Geotechnical and Geoenvironmental Engineering 131 (7), 826–836.

Gioda, G., Sakurai, A., 1987. Back analysis procedures for the interpretation of field measurements in geomechanics. International Journal of Numerical and Analytical Methods in Geomechanics 11 (6), 555–583.

Gordon, N.J., Salmond, D.J., Smith, A.F.M., 1993. Novel approach to nonlinear/non-Gaussian Bayesian state estimation. IEE Proceedings-F 140 (2), 107–113.

Higuchi, T., 2005. Particle filter, The journal of the institute of Electronics. Information and Communication Engineers 88 (12), 989–994 in Japanese.

Honjo, Y., Benny, L., Liu, W.T., 1993. Prediction of single pile settlement based on inverse analysis. Soils and Foundations 33 (2), 126–144.

Iizuka, A., Ohta, H., 1987. A determination procedure of input parameters in elasto-viscoplastic finite element analysis. Soils and Foundations 27 (3), 71–87.

Kalman, R.E., 1960. A new approach to linear filtering and prediction problems. Journal of Basic Engineering, ASME 82 (Series D), 35–45.

Karakus, M., Fowell, R.J., 2005. Back analysis for tunneling induced ground movements and stress redistribution. Tunnelling and Underground Space Technology 20 (6), 514–524.

Katayama, T., 1983. Applied Kalman filter. Asakura-shoten in Japanese.

Kitagawa, G., 1987. Non-Gaussian state-space modeling nonstationary time series. Journal of the American Statistical Association 82 (400), 1032–1041.

Kitagawa, G., 1996. Monte Carlo filter and smoother for non-Gaussian nonlinear state space models. Journal of Computational Graphical Statistics 5 (1), 1–25.

Kohavi, R., 1995. A study of cross-validation and bootstrap for accuracy estimation and model selection. International Joint Conference on Artificial Intelligence, 1137–1143.

Moral, P.D., Doucet, A., Jasra, A., 2006. Sequential Monte Carlo samplers. Journal of the Royal Statistics Society: Series B 68 (3), 411–436.

Murakami, A., Hasegawa, T., 1985. Observational prediction of settlement using Kalman filter theory. Proceedings of the 5th International Conference on Numerical Methods in Geomechanics, 1637.

Murakami, A., Hasegawa, T., 1987. Back analysis by Kalman filter-finite elements and a determination of optimal observed location. Proceedings of JSCE (388), 227–235 in Japanese.

Murakami, A. 1991: Studies on the application of the Kalman filtering to some geotechnical problems related to safety assessment. Doctoral Thesis, Kyoto University.

Murakami, A., Hasegawa, T., 1993. Application of Kalman filtering to inverse problems. Theoretical and Applied Mechanics 42, 3–14.

Nakai, T., Hinokio, M., 2004. A simple elasto-plastic model for normally and over consolidated soils with unified material parameters. Soils and Foundations 44 (2), 53–70.

Nakamura, K., Ueno, G., Higuchi, T., 2005. Data assimilation: concept and algorithm. Proceedings of the Institute of Statistical Mathematics 53 (2), 37–55 in Japanese.

Nakamura, K., Higuchi, T., Hirose, N., 2006. Sequential data assimilation: information fusion of a numerical simulation and large scale observation data. Journal of Universal Computer Science 12 (6), 37–55.

Nakano, S., Ueno, G., Higuchi, T., 2007. Merging particle filter for sequential data assimilation. Nonlinear Processes in Geophysics 14, 395–408.

Nakase, A., Kamei, T., Kusakabe, O., 1988. Constitutive parameters estimated by plasticity index. Journal of Geotechnical Engineering, ASCE 114 (7), 884.

Nishimura, S., Shimada, K., Fujii, H., 2002. Consolidation inverse analysis considering spatial variability and non-linearity of soil parameters. Soils and Foundations 42 (3), 45–61.

Nishimura, S., Nishiyama, T., Murakami, A., 2005. Inverse analysis of soft grounds considering nonlinearity and anisotropy. Soils and Foundations 45 (2), 87–95.

Rechae, C., Levasseur, S., Finno, R., 2008. Inverse analysis techniques for parameter identification in simulation of excavation support system. Computers and Geotechnics 35 (3), 331–345.

Sakurai, S., Takeuchi, K., 1983. Back analysis of measured displacement of tunnels. Rock Mechanics and Rock Engineering 16 (3), 173–180.

Schofield, A.N., Wroth, C.P., 1968. Critical State Soil Mechanics. McGraw-Hill.

Suzuki, M., Ishii, K., 1994. Parameter identification and probabilistic prediction of settlement of embankment. Structural Safety 14, 47–59.

Talagrand, O., Courtier, P., 1987. Variational assimilation of meteorological observations with the adjoint vorticity equation I: Theory. Quarterly Journal of the Royal Meteorological Society 113, 1311–1328.

Yumimoto, K., 2009. Data assimilation method with meteorological and chemical transport model. Nagare 28 (1), 37–44 in Japanese.